PCCP

Hydrogen Bonding Play a Significant Role in Binding of Coomassie Brilliant Blue-R to Hemoglobin: FT-IR, Fluorescence and Molecular Dynamics Studies

Journal:	*Physical Chemistry Chemical Physics*
Manuscript ID	CP-ART-08-2015-004661.R1
Article Type:	Paper
Date Submitted by the Author:	13-Oct-2015
Complete List of Authors:	Maiti, Nakul; Indian Institute of Chemical Biology, SBBD MAITY, MRITUNJOY; CSIR-Indian Institute of Chemical Biology, Division of Structural Biology and Bioinformatics Dolui, Sandip; CSIR-Indian Institute of Chemical Biology, Division of Structural Biology and Bioinformatics

Hydrogen Bonding Play a Significant Role in Binding of Coomassie Brilliant Blue-R to Hemoglobin: FT-IR, Fluorescence and Molecular Dynamics Studies

Mritunjoy Maity, Sandip Dolui and Nakul C Maiti*

Division of Structural Biology and Bioinformatics;
CSIR-Indian Institute of Chemical Biology;
4, Raja S.C. Mullick Road, Kolkata, India-700032;
Fax: (+) 91 33 24735197, 91 33 24723967; Tel: (+) 91 33 24995940

Received date:

* Address correspondence to Nakul C. Maiti, Division of Structural Biology and Bioinformatics, CSIR-Indian Institute of Chemical Biology, 4, Raja S.C. Mullick Road, Kolkata 700032

E-mail: ncmaiti@iicb.res.in

Phone: +91-33-2499-5940, +91-33-2473-5197/2472-3967

Abstract

An analog of coomassie brilliant blue R (CBB-R) recently found to act as an antagonist to ATP-sensitive purinergic receptors (P2X7R) and has potential to be used in medicine. With the aim of understanding its transportation and distribution through blood, in this investigation, we measured the binding parameters of CBB-R with bovine hemoglobin (BHG). The molecule specifically bound to single binding site of the protein with stoichiometric ratio 1:1 and the observed binding constants K_a were 3.5, 2.5, 2.0 and 1.5 x 10^5 M^{-1} at 20 ^oC, 27 ^oC, 37 ^oC and 45 ^oC, respectively. The measured respective ΔG^0 values of the binding in four temperatures were -30.45, -22.44, -18.04 and -11.95 kJ mol^{-1}. The ΔH^0 (change in enthalpy) and ΔS^0 (change in entropy) values were -23.6 kJ mol^{-1} and -70.66 J mol^{-1} respectively in the binding process. The negative value of ΔH^0 and ΔS^0 indicated that the binding of the molecule was thermodynamically favorable. The best energy structure in molecular docking analysis revealed that CBB-R preferred to be intercalated in the cavity among the α2, β1 and β2 subunits and the binding location was 7.4 Å far from Trp37 in the β2 subunit. The binding of the molecule with the protein was stabilized by hydrogen bonds involving side chain of two amino acid residues. The residues were Lys104, Glu101 in β2 subunit. The binding was further stabilized via hydrogen bond formation between amide group of peptide backbone (residue Tyr145 of β1 subunit) and CBB-R. A shift of amide I (-C=O stretching) band frequency of ~ 8 cm^{-1} to low energy was ascribed to the hydrogen bond interaction involving the polypeptide carbonyl of the protein and the CBB-R molecule. In addition, two π-cation interaction between Lys99 of α2 subunit and Lys104 of β2 subunit and CBB-R contributed

favorably in the binding processes. No substantial change in soret and 'Q' absorption bands of BHG could be observed in the presence of CBB-R. It indicated that the oxygen binding domain or the heme proximity was not blocked or substantially perturbed due to the binding of CBB-R. The circular dichroism and the molecular dynamic analysis further established that the binding interaction caused no significant alteration in the proteins long range secondary structure.

Key Words: coomassie, hemoglobin, FT-IR, thermodynamic parameter, fluorescence

List of abbreviations:

CBB-R: Coomassie brilliant blue R

BHG: Bovine hemoglobin

FT-IR: Fourier transform infrared spectroscopy

ATR-FT-IR: Attenuated total reflectance fourier transform infrared spectroscopy

MD: Molecular dynamics

CD: Circular dichroism

RMS: Root mean-square

UV-Vis: Ultra violet visible

RMSD: Root mean square deviation

R_g: Radius of gyration

1. INTRODUCTION

Coomassie brilliant blue R (CBB-R; chemical formula: $C_{45}H_{44}N_3NaO_7S_2$ (Figure 1), MW = 825.97) is an important triphenylmethane type dyes very similar to the commonly used blue food color and food additives (FD&C Blue No. 1, Brilliant Blue FCF). [1-3] The intense color of the molecule was due to its conjugated system spread over three rings and, the color largely depends on the pH of the solution. A unique presence of two sulfonic groups and three nitrogen atoms render CBB-R to produce this color and provides a configuration to interact with proteins and other macromolecules. In the interaction it is observed some changes in planarity of the conjugated ring moiety.[4, 5] The molecule prefers to bind basic amino acid residues and regions containing poly-(L-lysine), poly-(L-arginine), poly-(L-histidine), and poly-(L-ornithin).[6, 7] Affinity to protein molecules and its brilliant color producing ability was proved to be beneficial for protein detection method and it is used as a protein staining agent in SDS-PAGE electrophoresis.[8, 9] A recent study further showed that another analog of CBB-R (Coomassie brilliant blue G) could be used for the ATP-sensitive purinergic receptor, the P2X7 receptor (P2X7R) antagonist.[10] The excessive release of ATP by the traumatized tissue from the damage area of spinal cord injury, followed by the activation of the P2X7R causes the increase of Ca^{2+} ion concentration in the injured area, which makes the ultimate cell death. All these processes could be prevented by the P2X7R antagonist such as an analog of CBB-R[10-13]

Recent studies indicated that CBB-G250 shows significant affinity towards drug carriers proteins such as serum albumin proteins.[14] However a deeper understanding of the interaction is still much obscured. It is also not clear how it could bind other carrier proteins present in blood such as hemoglobin, myoglobin and others. In the current study, we investigated the binding behavior of the molecule with bovin hemoglobin (BHG).

Hemoglobin is a respiratory protein found in red blood cell in all vertebrates as well as in other living species like archaea, bacteria, fungi, protists and plants. Its well known function is to carry oxygen and carbon dioxide in between cell and respiratory system. The protein is a tetrameric form and composed of two identical α and β subunits, in which each subunit carries a heme group and oxygen binds reversibly and the binding is a cooperative process.[15] In addition, hemoglobin also acts as a carrier for other small molecules to deliver to different tissues. It also regulates the pH, nitric oxide and sulfide level. Because of its biocompatibility, biodegradability, usability and easy loading capability many drug molecules have attempted to design that may be carried out by hemoglobin. The studies also show different small molecule interaction and bind to this protein.[16-18] In the current investigation, we established how CBB-R binds to bovine hemoglobin (BHG) and demonstrated its binding site in the protein molecule. BHG composed of tetramer of myoglobin like unit and consists of two α and two β subunits which are non-covalently associated within erythrocytes with molecular weight 64.5 kDa.[19, 20] Earlier reports suggested that the heteropolyacid, various herbicides and favonoids interacts effectively with

hemoglobin.[21-23] Wang et al also showed that caffeine binds to the interface of the subunits.[24]

Several spectroscopic methods and techniques such as fluorescence, absorption and circular dichroism (CD) methods are used in studies metallo proteins and their interaction with different small molecules.[25, 26] In the current manuscript the binding interaction of CBB-R with bovine hemoglobin was studied by fluorescence, FT-IR and many other methods including molecular docking and dynamics simulation. Analysis of intrinsic protein fluorescence in the presence of ligand provides deeper understanding of binding mechanism, binding mode, binding constants, intermolecular distances and structure related information about the small molecule bound protein complex.[27]

Each αβ dimer of BHG contains three tryptophan (Trp) residues, one in each α-subunit and two in each β-subunit, so for a total six Trp residues, two α-14 Trp, two β-15 Trp, and two β-37 Trp are located.[28, 29] Although there are six Trp residues, the intrinsic emission is very weak due to the tryptophan-heme energy transfer and R-T structural transitions in hemoglobin.[30] Among the three Trp residues in each dimer subunit, only β-37 Trp residue holds the key role for intrinsic fluorescence of hemoglobin.[31, 32] The interaction of any foreign ligand with β-37 Trp alters the fluorescence behavior.[33] In this study we measured parameters linked to binding of CBB-R to BHG by utilizing the fluorescence in the absence and presence of the molecule in the protein solution. In addition, molecular modeling and dynamics - analysis assisted to locate the binding site, its specificity and the type of interacting forces. We showed residue specific hydrogen bonding interaction and their stability in

different time frame in the protein micro-environment. An investigation by circular dichroism (CD) spectroscopy further established that the binding of the molecule caused no major changes in the protein secondary structure.

2. MATERIALS and METHODS

Chemicals

All chemicals used in this investigation were of analytical grade or of the highest purity available. BHG (lyophilized powder) and CBB-R were purchased from Sigma-Aldrich. Disodium hydrogen phosphate (Na_2HPO_4) and sodium dihydrogen phosphate monohydrate (NaH_2PO_4, H_2O) was purchased from Merck Millipore. All reagents were used as received. Mill-Q water was used to prepare all the solutions in this study.

Absorption spectroscopy

Absorption spectra of all the samples for this study were measured with a JASCO V-630 Spectrophotometer (JASCO International Co. Ltd, Japan) in the range of 230 to 800 nm wavelength. High quality quartz cuvette was used to record the spectra. The concentration of BHG was 5×10^{-6} mol/L.

FT-IR spectroscopy

The FT-IR spectra of the samples were recorded on a Bruker TENSOR27 spectrometer using liquid state techniques. The liquid samples (CBB-R or BHG) were mixed with 5mM phosphate buffer at pH 7.4 in a clean glass bottle and kept for three minutes at room temperature. The spectra were recorded from 400–4000 cm^{-1}. Background spectra were obtained with above phosphate buffer for each sample. Bruker software was used for data processing. The strong peaks in the spectra were reproducible and appeared each time within ± 3 cm^{-1}.

Fluorescence spectral measurements:

The Intrinsic tryptophan fluorescence of the BHG and CBB-R were recorded with an Agilent Technology, Cary Eclipse fluorescence spectrophotometer equipped with Xenon lamp and a quartz cell (4cm × 1cm × 1cm). The excitation slit was 10 nm and emission slit was 20 nm. The excitation wavelengths and emission measurement were selected according to the sample. All the fluorescence measurements were made after 10 min of incubation CBB-R with BHG solutions. Fluorescence measurements were repeated at least three times for each sample. Synchronous intrinsic fluorescence spectra were measured by simultaneously scanning the excitation and emission monochromator in the excitation wavelength range 250–400 nm with a constant difference between excitation and emission wavelength $\Delta\lambda$= 60 nm between them. Fluorescence spectra were plotted as a function of the excitation wavelength Windows-based software OriginPro 7.5 (OriginLab, USA, 2002) was used for the plotting purposes.

Circular Dichroism (CD):

Circular Dichroism (CD) measurements were conducted on a JASCO J-815 spectropolarimeter equipped with the PFD-425 Peltier temperature control. All the CD measurements were performed at the 25 ^{o}C with accuracy of ±0.1 ^{o}C. Spectra were collected with a scan speed of 100 nm min^{-1} and with a spectral bandwidth of 1.00 nm. Each spectrum was the average of three scans. Secondary structure (Far-UV CD) was measured over the wavelength range of 190-250 nm using a 1 mm path

length curvature.[34] Each represented spectra were average of three individual scans. For all the measurement the protein concentration of 2.0 μM was used.

Molecular docking studies:

The docking experiments were performed using AutoDock4.2 and AutoDock Tools 1.5.4 (ADT).[35] A Lamarckian generic algorithmic method, implemented in the program AutoDock 4.2 was employed to identify appropriate binding modes and conformations of the ligand.[36] The known crystal structure of BHG (PDB ID: 1G09) was obtain from the protein data bank. CBB-R constructed by chemdraw software, and optimized at the B3LYP/6-31G(d) level using the Gaussian 09 program.[37] The Gasteiger charges were assigned to BHG and the non-polar hydrogen atoms were merged using Auto Dock Tools. BHG was held rigid and all the torsional bonds of CBB-R are taken as being free during the docking calculations. To recognize the binding sites in BHG, blind docking was carried out, the grid size set to 126, 126 and 126 along the X, Y, and Z-axis with 0.0375 nm grid spacing. The docking parameters used were GA population size 150, maximum number of energy evaluation: 25, 0000. During the docking process, a maximum of 100 conformers was considered for each compound. The root mean-square (RMS) cluster was set to 2.0 Å in each run. The output from AutoDock is rendered with PyMOL.[38] Here, PyMOL has also been used to calculate the distances between nearest atoms which interact with each other.

Molecular dynamic simulation

A molecular dynamics simulation of the best energy docking conformation BHG-CBB-R complex was carried out through Desmond.[39, 40] Force field parameters for the BHG/CBB-R complex were set using OPLS 2005 molecular mechanics force field and this complex surrounded by a cubic box contain spc water solvent model and the cubic box dimension is 105 x 105 x 105 Å.[41 42] The System was neutralized by adding a number of counter ions. SHAKE algorithm was used to constrain the geometry of covalent bonds involved hydrogen atoms. The energy of prepared systems for MD simulations was minimized up to a maximum of 5000 steps using a steepest descent method until a gradient threshold (25 kcal mol^{-1} A^{-1}) was reached, followed by LBFGS (Low-memory Broyden-Fletcher-Goldfarb-Shano quasi-Newtonian minimize) algorithm with maximum 2000 iterations. Non hydrogen atoms were restrained with an NVT ensemble (temperature 10 K) using 12 picoseconds (ps) simulation time. The similar MD simulation was then carried out for NPT ensemble. The pressure and temperature of the whole system were controlled by a Berendsen thermostat and berostat. The BHG/CBB-R complex was stimulated for 40 ns with NPT ensemble using a Nose-Hoover chain thermostat at 300 K and Martyna-Tobias-Klein barostat at 1.013 bar pressure. The energy data of the complex were recorded every 1.2 ps and the atomic coordinate trajectory data of the complex were recorded every 4.8 ps. [43, 44]

3. RESULT and DISCUSSION

The binding interaction of CBB-R with BHG at pH 7.4 was measured via absorption, fluorescence and other spectroscopic methods. Figure 2 shows the absorption spectra of BHG in 10 mM phosphate buffer at pH 7.4 in the absence and presence of different concentration of CBB-R. The soret band of porphyrin moiety in BHG molecule appeared at ~405 nm. There was no significant change in the soret band position in the presence of different concentration of CBB-R in the protein solution. The 'Q' bands were also not significantly affected. It indicated that the oxygen binding domain or the heme proximity was not the active binding site and there might be no direct interaction between CBB-R and porphyrin moiety. It was also confirmed by molecular dynamics study, as discussed later, that the binding of CBB-R to BHG did not perturb significantly the oxygen binding region.[45] CBB-R also has a strong absorption in UV-Vis region. Hence, the consecutive addition of the molecule to the protein solution, the absorption band at ~ 600 nm was sequentially increased (Figure 2B).

Along with absorption, intrinsic tryptophan fluorescence of BHG was also measured in the presence of several concentrations of CBB-R. Figure 3 shows fluorescence spectra of BHG (5μM) solution containing different amounts of CBB-R. The fluorescence of the protein arises due to the emission from tryptophan residues and the fluorescence peak appeared at ~ 328 nm upon excitation at 290 nm. Among several Trp residues the fluorescence emission of BHG primarily originates from β-Trp37.[31, 32] A significant quenching of the protein fluorescence at 328 nm occurred in

the presence of CBB-R. The plot of F_0/F against the quencher concentration did not show any downward turn and indicated that there was no more than one significant population of fluorophore (tryptophan) in the system (Figure S3).

Figure 3 shows the gradual decrease of the intrinsic tryptophan fluorescence upon addition of different amount of CBB-R. This indicated considerable binding interaction of the molecule with the protein. CBB-R itself showed some fluorescence and the band appeared at 366 nm (Figure S1). The fluorescence contribution from the CBB-R at 330 nm was very minimal (as shown in Figure S1).[46] However, CBB-R fluorescence contribution to the protein emission was corrected (described in the supporting material). The absorbance of CBB-R was minimum at the emission of protein, but some contribution at an excitation wavelength of protein was observed. Therefore the inner filter effect correction was made on the acquired spectra using the following equation 1.

$$\mathbf{F_{corr} = F_{obs}\ X\ antilog}\left(\frac{\mathbf{A_{ex} + A_{em}}}{\mathbf{2}}\right) \quad \text{.....(1)}$$

Where F_{corr} and F_{obs} are the corrected and observed fluorescence intensity, respectively. A_{ex} and A_{em} are the absorbance of CBB-R at excitation (290 nm) and emission wavelength (330 nm), respectively.[33] The corrected spectra showed that fluoresce could be quenched more than 80% by the molecules. Figure 3B and figure S2 shows the corrected fluorescence spectra of BHG in the presence of different concentration of CBB-R.

To measure the apparent dissociation constant (K_d) of CBB-R binding to BHG a modified stern-volmer equation (Equation 2) (Lakowicz 2006, 3rd edition, p. 289)[47] was fitted to the corrected fluorescence intensity at 328 nm of the BHG solution in the presence of different concentration of CBB-R (Figure 4A).

$$\mathbf{F_0/\Delta F = 1/ (}f K_a \mathbf{[Q]) + 1/}f \quad \text{..... (2)}$$

Where F_0 is the initial fluorescence intensity in the absence of CBB-R, ΔF is the difference in fluorescence in the absence and presence of the CBB-R at a concentration [Q], K_a is the stern-volmer quenching constant, and f is the fraction of the initial fluorescence which is accessible to the quencher (Lakowicz 2006). The plots of $F_0/\Delta F$ versus 1/[Q] yield f^{-1} as the intercept and $(f K_a)^{-1}$ as the slope. The measured stern-volmer quenching constants, using the modified S–V equation can be expressed as binding affinity constant, K_a.[33, 48] The reciprocal of K_a gives the dissociation constant, K_d. The values of K_a were $3.5 \times 10^5\ M^{-1}$, $2.5 \times 10^5\ M^{-1}$, $2.0 \times 10^5\ M^{-1}$ and $1.5 \times 10^5\ M^{-1}$ at 20 °C, 27 °C, 37 °C and 45 °C, respectively. The calculated K_d values at different temperatures were 2.84, 4.00, 4.91 and 6.36 μM at 20 °C, 27 °C, 37 °C and 45 °C, respectively.

The fluorescence quenching of a fluorophore is induced by the different types of interaction between fluorophore and a quencher molecule (CBB-R) such as energy transfer, collision, excited-state reaction, molecules rearrangement and ground state complex formation. These all belongs one of the two classes of fluorescence quenching mechanisms: (I) dynamic fluorescence quenching and (II) static

quenching. Dynamic fluorescence quenching processes occurs primarily via a collision process and the diffusion play a key role in the magnitude of the quenching.[49] The solvent viscosity and size of the quencher play vital roles in diffusion and on the extent of quenching. On the other hand, the close association of the fluorophore and the quencher lead to decrease of fluorescence mainly involved in static mechanism.

The static and dynamic quenching can often be distinguished by measurement of fluorescence lifetime of a protein in the presence of quencher. In a dynamic quenching procees the fluorescent lifetime decreases and in static quenching the apparent concentration of the fluorophore (tryptophan) becomes less, however fluorescence lifetime remains quite similar. In the static method often complex formation occurred and the strengths of its often varied inversely with temperature. On the contrary, in the dynamic quenching, being it diffusion controlled the quenching rates, increase in temperature and the fluorescence lifetime decreases. The lifetime measurements of BHG tryptophan fluorescence were performed both in the presence and absence of the CBB-R. Table TS1 shows the average fluorescence lifetime of the protein and it was similar to the value reported earlier.[50] Tryptophan is known to show multi-exponential fluorescence decay, however, we have not tried to identify the individual components; conversely, the average lifetime was determined in order to acquire a qualitative analysis. The average lifetimes (τ) computed from the decay parameters remained essentially unchanged. This indicated that a static mechanism is principally responsible for the observed steady-state fluorescence quenching when CBB-R binds and interact with bovine hemoglobin (BHG). We also

observed that steady state fluoresce quenching was higher at lower temperature (Figure 4A). Thus the lifetime results and temperature dependent study indicated that the fluorescence quenching mainly followed static quenching mechanism.

Measurement of thermodynamic parameters and nature of binding force

Temperature dependent fluorescence quenching was performed to obtain the K_d values at several temperatures and the thermodynamic parameters of binding were determined by fitting the van't Hoff's equation (equation 3) to fluorescence data. The plot is shown in Figure 4B.

$$\ln K_a = -\Delta H^0/RT + \Delta S^0/R \quad \text{..... (3)}$$

Where K_a is the equilibrium constant (here the stern-volmer quenching constant) of binding at a corresponding temperature (K) and R is the universal gas constant (8.314 J $K^{-1}mol^{-1}$). The obtained standard enthalpy change (ΔH^0) and entropy change (ΔS^0) on binding are given in Table 1. The free energy change (ΔG^0) was estimated using equation (4) and the values are given in Table 1.

$$\Delta G^0 = \Delta H^0 - T\Delta S^0 \quad \text{..... (4)}$$

The measured ΔG^0 for the binding process was -20.72 kJ mol^{-1} (average of all four temperatures). The negative ΔG^0 value indicated that the binding was spontaneous processes and thermodynamically favorable. Both the ΔH^0 and ΔS^0 were also negative. The negative values for ΔG^0, ΔH^0 and ΔS^0 indicated that the van der Waals force and H-binding type of interaction may significantly contribute to the stability of the BHG/CBB-R association.[51, 52]

The number of binding sites of the protein with ligands was calculated from fluorescence quenching data obtained at four different temperatures (Figure 5). The fluorescence intensity in the presence of different concentration of CBB-R was fitted with the Scatchard equation (equation 5).

$$\log\left(\frac{F_0 - F}{F}\right) = \log K + n \log[Q] \quad \text{..... (5)}$$

where n is the number of binding sites in each BHG molecule, [Q] is the molar concentration of CBB-R and *K* is the equilibrium binding constant.[53] Figure 5 displays a linear plot of log $[(F_0-F)/F]$ versus log [Q]. The number of binding sites (n) was obtained from the slope of the fitted straight line and listed in Table 1.

To measure the binding proximity of CBB-R and Trp that produces fluorescences synchronous spectra of BHG were measured by simultaneous scanning the excitation and emission monochromater and maintained the $\Delta\lambda$ (difference between excitation and emission wavelength) of 60 nm (Figure 6).[54] The plot shows that the excitation peak of Trp emission was red shifted about 4 nm due to binding of CBB-R to the protein. The red shift indicated that the polarity around the tryptophan residues was increased to some extent. This may be due to the changes of residue micro-environment with the insertion of CBB-R. Our docking result, as discussed below, revealed that CBB-R binding site was ~ 7.4 Å away from Trp37 of β1 subunit of the protein molecule.

FT-IR study

FT-IR spectroscopy is one of the well defined and versatile techniques often used for the determination of protein's secondary structure and their interaction with small molecules and other ligands in diverse physiochemical conditions.[15, 55-59] Figure 7A and 7C shows FT-IR spectra of the protein in aqueous solution in the absence and presence of CBB-R, respectively. In all the cases FT-IR bands between 700-2000 cm^{-1} are shown. The significant FT-IR bands of both the protein and ligand are marked in the figures. The band positions were assigned based on available information in the literatures.[57, 60-62 63] The spectrum of the CBB-R molecule alone is shown in figure 7B. Solid state FT-IR spectra of both the BHG and CBB-R are shown in figure S4 and S5, respectively.

The major structural information of a protein from FT-IR spectra is obtained from amide I band position which appeared in 1600-1700 cm^{-1}. The band is ascribed largely C=O stretching vibrations of the peptide bond in a polypeptide chain. A strong band at 1652 cm^{-1} (solid state, Figure S4) was due to amide I mode vibration and the band was assigned to major α-helical structure of BHG.[64] The band was shifted to 1648 cm^{-1} in aqueous buffer solutions (Figure 7A). The amide II bands of free protein appeared at 1546 cm^{-1} in the solution state (in the solid state the band appeared 1539 cm^{-1}). The bands at 1310 and 1245 cm^{-1} well could be assigned to amide III vibrations. In the proteins polypeptide backbone the N-H stretching vibration appears as amide A and B bands between 3300 and 3250 cm^{-1}. BHG in the buffer solutions showed a band at 3278 cm^{-1} (in the solid state 3277 cm^{-1}). This band could be due to the contribution of NH vibration (amide A). However, the frequency

associated with this band highly dependent on the strength of hydrogen bond it form with the surrounding molecules and solvents. The amide B band appeared at ~2985 cm^{-1}. The methylene group $–CH_2$- usually gives a band around 2850 cm^{-1} and the protein in solid state showed a band at 2874 cm^{-1} (in solution 2882 cm^{-1}) which was a possible candidate for the above vibration.

CBB-R showed a number of absorption peaks in FT-IR spectra and these were due to different vibrations of aromatic ring, aliphatic groups (-CH_2, -CH_3) and functional groups (-NH, -SO_3H and -$SO3^-$). The FT-IR spectrum of solid CBB-R is shown in Figure S5 and the solution state FT-IR spectrum of the molecule is shown in Figure 7B. The major vibration bands in solid state were observed at 3436, 3255, 2969, 2927, 1580, 1510, 1412, 1368, 1343, 1296, 1226, 1169,1112, 1037, 1075, 911, 829 and 615 cm^{-1}. The band in the region between 3122-3680 cm^{-1} were originated mainly due to hydroxyl (-OH) groups stretching motion. 3436 cm^{-1} attributed to the –OH stretching vibrations of $–SO_3H$ group. The band at 2969 and 2927 cm^{-1} represented the presence of alkanes groups. In the solution state we observed a broad band at ~ 3443 cm^{-1} due to the –OH (-SO_3H) vibration. Possible aromatic skeletal vibrations appeared at 1580 and 1412 cm^{-1} and in solution the band shifted to 1583 cm^{-1} observed. The vibration bands at 1037 cm^{-1} could be due to sulfoxide (S=O) stretching mode and 1368 cm^{-1} stretching in SO_3H. The band at 2969 and 1510 cm^{-1} suggest the presence of possible CH_2 stretching and bending, respectively.

The amide I band was noticed to be shifted from 1648 cm^{-1} (in free BHG) to 1640 cm^{-1} in the BHG/CBB-R complex. Amide I band arises mainly due to the C=O stretching vibration. However, some minor contributions come from the out-of-phase

C≡N stretching motion. C-C-N deformation and the N-H in-plane bending motion also contribute to the band to some extent. The amide II marker band was at 1545 cm^{-1} in the complex. No significant change was observed in this band. The origin of the amide II bands is due to C–N stretching coupled with N–H bending mode. The lowering of C=O stretching in amide I mode occurs due to weakening of the average carbonyl group in the peptide bond. The weakening of the bond and the resulting shift in the amide I frequency of a protein depends on peptide backbone conformation.[56] In addition interaction such as hydrogen bond formation with water or ligands may also cause measurable shift in the amide I band vibration frequency of protein molecule.[65] The molecular vibration frequency depends on its bond length and strength (force). Hydrogen bonding in general however, lowers stretching frequency of carbonyl group (C=O) as it lowers the restoring force that. The same phenomenon may increase the frequency of bending vibrations since it adds some amount of additional restoring force.[66]

In our investigation, we observed that amide I mode frequency was 8 cm^{-1} shifted to lower frequency range. However, there were no major changes in the amide II vibration mode in the BHG/CBB-R complex. It indicated that some hydrogen bond formation between the protein backbone carbonyl and CBB-R/water caused these changes in the frequency. In model compound studies it was observed that the carbonyl stretching vibration may be reduced 20 cm^{-1} due to formation of a C=O group of methylacetate with water.[67-69] Several reports further show a linear relationship between the enthalpy of hydrogen bond formation (ΔH) and the change in frequency of the stretching vibration.[65, 70-74] It is known that the carbonyl group of

methyl acetate which is often used as a model for Lys and Glu, showed ~ 1 cm^{-1} shift to low frequency of the C=O stretching with a favorable binding enthalpy of 1.7 kJ mol^{-1}. [58, 74 65] As discussed below, the lowest energy docked model suggests one hydrogen bonding possibility in case of CBB-R and BHG, namely between the C=O of the peptide linkage involving Tyr145 (β1 subunit) of BHG and NH group of CBB-R. We observed ~8 cm^{-1} change in the amide I band frequency when CBB-R bound to the protein. Using the above mentioned relationship, the calculated energy contribution was ~ 13.6 KJ Mol^{-1}. From fluorescence quenching results the obtained ΔH was -23.6 kJ mol^{-1}. Additional stability the complex may gain from other interaction, such as π-cation interaction as explained in the molecular dynamic analysis. It has also been shown by Raman studies that C=O groups of substrates bound to enzymes showed considerable shift in frequency due to water binding via hydrogen bonding in the complex.[75] Our investigation did not focous how the general hydration lavel of the protein backbone changed upon the binding of CBB-R to the protein, however, synchronous emission (Figure 6) mesurment indicated increase in polarity surrounding the Trp37 and therefore it could be possible that some contribution from hydrogen bond formation of C=O bond with the water caused the red shift in the amide I bond vibration. Both the molecular dynamic analysis and the CD studies also indicated no significant perturbation of the protein secondary structure. Thus the shift in the C=O stretching frequency well could be correlated to the formation of one hydrogen bond interaction between CBB-R and the protein backbone.[65, 76]

Circular dichroism spectra study

To investigate the possible influence of CBB-R on the secondary structure of BHG, we have performed far-UV circular dichroism spectroscopy of BHG in the absence and in the presence of CBB-R. Figure 8 displays the CD spectra of BHG in the presence of several concentrations of CBB-R. The addition of the CBB-R into BHG solution did not cause large perturbation of the UV-region CD spectrum. It indicated no long changes in the protein secondary structure upon due to CBB-R binding to the protein.[77]

Computational study

Molecular docking

Molecular docking and dynamic analysis indicated that H-bonding interaction between specific amino acid residues and CBB-R plays a significant role in the event of binding of CBB-R molecule to the protein. For the docking of CBB-R to BHG the best energy conformer of the molecule was chosen out of 100 different conformers (Figure 1, right). The ΔG^0 value of best energy conformer as docked was -22.99 kJ mol^{-1}. The best energy structure revealed that CBB-R located near the cavity of BHG generated by three subunits α2, β1 and β2 (Figure 9A). It is well-known that hemoglobin has two binding site: site-I is present between α2 and β1 subunits may be suitable for the binding of electronegative ligands and site-II present near the α1 subunit contributes to electropositive ligands binding.[33] It was observed that CBB-R was preferably binds to site-I and stabilized by hydrogen bond interaction with

Tyr145 of β1 subunit, Lys104 and Glu101 of β2 subunit of the protein. The two π-cation interactions were also observed with Lys99 of α2 subunit (Figure 9B).

Molecular dynamics

Molecular dynamics (MD) simulation was often carried out to clarify the conformational changes of proteins and the stability of the complex in the event of small molecule binding to the protein. The MD stimulation was carried out for 40 ns with both the unbound BHG and the complex (BHG/CBB-R) of lowest energy structure in water. The dynamic structural properties (RMSDs and radius of gyration (Rg)) of free BHG and BHG/CBB-R complex were analyzed to measured the stability and compactness.

The MD simulation results revealed that the root mean square deviation (RMSD) provides insights of protein conformation throughout the simulation; it also indicated that the simulation has equilibrated or its fluctuations towards the end of the simulation are around some thermal average structure. The RMSD values of atoms of free BHG and complex BHG/CBB-R with respect to initial structures have been calculated along the 0 to 40000 ps trajectories as shown in Figure 11. It should be noted that two trajectories have RMSD values within 0.8-2.4 Å during 40000 ps simulation. For free BHG system, the RMSD value is 1.6 Å at 22894 ps. After this, the value is increased up to 2.4 Å. In case of the BHG/CBB-R complex, the RMSD values show a similar trend to free BHG up to 6492 ps. After this there is no additional increase of RMSD values up to 22950 ps and the complex system reaches equilibrium. After 29460 ps, the BHG/CBB-R complex system shows lower RMSD

value than the free BHG system. The decrease in the RMSD value of the complex system from that of the free BHG system signified increased rigidity and stability of BHG binding with CBB-R.

A similar structural envelope was obtained from the variation in the radius of gyration (R_g) of the protein. The radius of gyration provides a rough estimate of the compactness of a protein structure. The radius of gyration of both free BHG system and BHG/CBB-R complex system has been determined and plotted as a function of time (Figure 12). During the stimulation time trajectory, the average R_g of the bound complex was 23.8 Å and the free BHG was 23.6 Å. The similarity of R_g values of the free protein and complex signified almost unchanged secondary structure of the protein. We did not find much structural changes in the BHG structure due to CBB-R binding from the MD simulation and circular dichroism studies.

The intermolecular hydrogen bond between protein and ligand plays a significant role in stabilizing the protein-ligand complexes.[78] We performed H-bond analysis to find out distance between the CBB-R and interaction amino acid residus of BHG. We observed during docking simulation three H-bond interactions form with two side chain residues Lys104, Glu101 of β2 subunit and one backbone Tyr145 residue of β1 subunit. During 40 ns of MD simulation, we observed that two stable H-bonds are formed between Tyr145 of β1 subunit and Asp99 of β2 subunit of BHG and CBB-R (Figure 13, S7). Here, one H-bond with Asp99 of β2 subunit of BHG was newly formed during MD simulation (Figure S7). We also showed the distances of two stable H-bond after 40 ns of MD simulation (Figure S8).

These numbers H-bonding indicated that binding of CBB-R stabilized the protein system. A Trp residue has a significant contribution toward the fluorescence of protein. BHG contain 6 Trp residues, Trp37 at the β interface is a significant contributor of intrinsic fluorescence emission.[31, 32] Results obtained by molecular docking and dynamic analysis indicated that the distance of bound CBB-R from the Trp residue was ~9.5 Å (as observed for 40 ns molecular dynamics analysis, Figure 14 and Figure S10). For excited state energy transfer distance between fluorophore and the quencher varied between 1 nm (10 Å) to 9 nm (90 Å). The measured distance of ~9.5 Å is therefore significant for energy transfer.[33, 79] The CBB-R presents very close to the Trp37 of β2 subunits, evident from the docking study (Figure 10). During the MD simulation, distance of CBB-R slightly increases to ~ 9.5 Å away from the Trp37 residue (Figure 14 and Figure S10).

Another significant feature that appeared from MD simulation was the distance between CBB-R and the iron atoms of the heme moieties. Figure 15 displays the projection of CBB-R binding to BHG. The nearest distance of CBB-R to any of the four Fe atoms was 16 Å. This observation indicated that the CBB-R did not hamper oxygen binding of hemoglobin, the condition which was also observed in the absorption spectra where soret band of the protein was similar in the presence of CBB-R.

CONCLUSION

The significance of the present work lies in the fact that hemoglobin is a natural drug carrier in physiological systems and CBB-R favorably binds at the interface of several subunits present in the protein. The study also suggested that the binding interaction caused no significant alteration in the proteins long range secondary structure. Importantly the binding of the molecule to the protein did not prefer the heme binding site and thus it may not hamper the proteins important function of oxygen transportation. An analog of the molecule (CBB-R) was recently found to act as an antagonist to ATP-sensitive purinergic receptors and our observation were that the molecule specifically could bind to this oxygen carrier protein without effecting the oxygen binding site. Absorption and molecular docking and dynamics analysis all showed that the oxygen binding domain or the heme proximity was not blocked or substantially perturbed due to the binding of CBB-R. This information may have significant implication in understanding the pharmacokinetics of similar other molecules including its own derivatives.

Acknowledgements

We thank Council of Scientific and Industrial Research (CSIR), India, for the fellowship to M. Maity (31/002(0897)/2011-EMR-I) and S. Dolui (Senior Project Fellowship, from CSIR-IICB). The authors also thank Prof. Nikhil Guchhait, University of Calcutta for providing TCSPC facility for lifetime measurement. We also thank Prof. Achintya Saha, University of Calcutta for providing some support in computational studies. We gratefully acknowledge the grant supports, BSC-0113, CSIR-IICB and GAP-299 from the Department of Biotechnology, government of India. Mr. Uttam Pal read the manuscript and we particularly appreciate his comments on computational work.

Table 1: Modified Stern-volmer quenching constant (K_a), dissociation constant (K_d) and thermodynamic parameters of BHG/CBB-R complex

Temperature (K)	K_d **(μM)**	K_a **(M^{-1})**	**Number of binding sites (n)**	ΔG^0 **(kJ mol^{-1})**	ΔH^0 **(kJ mol^{-1})**	ΔS^0 **(J mol^{-1})**
20 ^oC	2.84	3.51 x 10^5	1	- 30.45	-23.6	-70.66
27 ^oC	4.00	2.49 x 10^5	1	- 22.44		
37 ^oC	4.91	2.03 x 10^5	1	- 18.04		
45 ^oC	6.36	1.57 x 10^5	1	-11.95		

References

1. S. M. Hess and O. G. Fitzhugh, *J. Pharmacol. Exp. Ther.*, 1955, **114**, 38-42.
2. M. Remy, S. Thaler, R. G. Schumann, C. A. May, M. Fiedorowicz, F. Schuettauf, M. Gruterich, S. G. Priglinger, M. M. Nentwich, A. Kampik and C. Haritoglou, *Br J Ophthalmol*, 2008, **92**, 1142-1147.
3. J. F. Borzelleca, K. Depukat and J. B. Hallagan, *Food Chem. Toxicol.*, 1990, **28**, 221-234.
4. H. J. Chial, H. B. Thompson and A. G. Splittgerber, *Anal. Biochem.*, 1993, **209**, 258-266.
5. A. G. Splittgerber and J. Sohl, *Anal. Biochem.*, 1989, **179**, 198-201.
6. I. Wittig, H.-P. Braun and H. Schaegger, *Nat. Protoc.*, 2006, **1**, 418-428.
7. S. F. d. S. Groth, R. G. Webster and A. Datyner, *Biochim. Biophys. Acta*, 1963, **71**, 377-391.
8. M. M. Bradford, *Anal. Biochem.*, 1976, **72**, 248-254.
9. H. Schagger and J. G. von, *Anal Biochem*, 1991, **199**, 223-231.
10. D. Erlinge and G. Burnstock, *Purinergic Signalling*, 2008, **4**, 1-20.
11. G. Collo, S. Neidhart, E. Kawashima, M. Kosco-Vilbois, R. A. North and G. Buell, *Neuropharmacology*, 1997, **36**, 1277-1283.
12. X. Wang, G. Arcuino, T. Takano, J. Lin, W. G. Peng, P. Wan, P. Li, Q. Xu, Q. S. Liu, S. A. Goldman and M. Nedergaard, *Nat. Med. (N. Y., NY, U. S.)*, 2004, **10**, 821-827.
13. W. Peng, M. L. Cotrina, X. Han, H. Yu, L. Bekar, L. Blum, T. Takano, G.-F. Tian, S. A. Goldman and M. Nedergaard, *Proc. Natl. Acad. Sci. U. S. A.*, 2009, **106**, 12489-12493, S12489/12481-S12489/12484.
14. Y.-S. Li, Y.-S. Ge, Y. Zhang, A.-Q. Zhang, S.-F. Sun, F.-L. Jiang and Y. Liu, *J. Mol. Struct.*, 2010, **968**, 24-31.
15. S. Nakashima, T. Ogura and T. Kitagawa, *Biochim. Biophys. Acta, Bioenerg.*, 2015, **1847**, 86-97.
16. P. D. Patel, N. Dand, R. S. Hirlekar and V. J. Kadam, *Curr. Pharm. Des.*, 2008, **14**, 63-70.
17. M. Hamidi, H. Tajerzadeh, A.-R. Dehpour, M.-R. Rouini and S. Ejtemaee-Mehr, *Drug Delivery*, 2001, **8**, 223-230.
18. T. Adams, F. Alanazi and D. R. Lu, *Curr. Pharm. Biotechnol.*, 2003, **4**, 275-282.
19. R. I. Weed, C. F. Reed and G. Berg, *J. Clin. Invest.*, 1963, **42**, 581-588.
20. M. L. Doyle, J. M. Holt and G. K. Ackers, *Biophys. Chem.*, 1997, **64**, 271-287.
21. Y.-Q. Wang, H.-M. Zhang and G.-C. Zhang, *Wuji Huaxue Xuebao*, 2006, **22**, 895-899.
22. B. Bukowska, E. Reszka and W. Duda, *Biochem. Mol. Biol. Int.*, 1998, **45**, 47-59.
23. S. Chaudhuri, S. Chakraborty and P. K. Sengupta, *Biophys. Chem.*, 2011, **154**, 26-34.
24. Y.-Q. Wang, H.-M. Zhang and Q.-H. Zhou, *Eur. J. Med. Chem.*, 2009, **44**, 2100-2105.

25. N. Abdullah, B. Srinivasan, N. Modiano, P. Cresswell and A. K. Sau, *Journal of Molecular Biology*, 2009, **386**, 690-703.
26. Z. L. a. K. S. A. Apurba Kumar Sau, *The Journal of Biological Chemistry*, 2003, **279**, 15787-15794.
27. A. Kumar Sau, D. Currell, S. Mazumdar and S. Mitra, *Biophysical Chemistry*, 2003, **106**, 233-240.
28. M. F. Perutz, *Nature (London)*, 1970, **228**, 726-734.
29. M. F. Perutz, A. J. Wilkinson, M. Paoli and G. G. Dodson, *Annu. Rev. Biophys. Biomol. Struct.*, 1998, **27**, 1-34.
30. B. Alpert and R. Lopez-Delgado, *Nature (London)*, 1976, **263**, 445-446.
31. M. F. Perutz, *Nature*, 1970, **228**, 726-739.
32. R. E. Hirsch, R. S. Zukin and R. L. Nagel, *Biochem. Biophys. Res. Commun.*, 1980, **93**, 432-439.
33. M. Banerjee, A. Chakrabarti and S. Basu, *Dyes and Pigments*, 2013, **97**, 446-454.
34. T. J. J. Sharon M. Kelly, Nicholas C. Price, *Biochimica et Biophysica Acta* 2005, **1751**, 119-139.
35. G. M. Morris, D. S. Goodsell, R. S. Halliday, R. Huey, W. E. Hart, R. K. Belew and A. J. Olson, *J. Comput. Chem.*, 1998, **19**, 1639-1662.
36. G. M. Morris, R. Huey, W. Lindstrom, M. F. Sanner, R. K. Belew, D. S. Goodsell and A. J. Olson, *J Comput Chem*, 2009, **30**, 2785-2791.
37. Y. Bai, J. Du and X. Weng, *Spectrochim. Acta, Part A*, 2014, **126**, 14-20.
38. D. Seeliger and B. L. Groot, *J. Comput.-Aided Mol. Des.*, 2010, **24**, 417-422.
39. V. Gomathi Sankareswari, D. Vinod, A. Mahalakshmi, M. Alamelu, G. Kumaresan, R. Ramaraj and S. Rajagopal, *Dalton Trans.*, 2014, **43**, 3260-3272.
40. Z. Guo, U. Mohanty, J. Noehre, T. K. Sawyer, W. Sherman and G. Krilov, *Chem. Biol. Drug Des.*, 2010, **75**, 348-359.
41. D. Shivakumar, J. Williams, Y. Wu, W. Damm, J. Shelley and W. Sherman, *J. Chem. Theory Comput.*, 2010, **6**, 1509-1519.
42. T. Sindhu and P. Srinivasan, *Mol. BioSyst.*, 2015, **11**, 1305-1318.
43. Y. Yang, J. Qin, H. Liu and X. Yao, *J. Chem. Inf. Model.*, 2011, **51**, 680-692.
44. S. K. Tripathi, R. Muttineni and S. K. Singh, *J. Theor. Biol.*, 2013, **334**, 87-100.
45. P. Ormos, S. Szaraz, A. Cupane and G. U. Nienhaus, *Proc. Natl. Acad. Sci. U. S. A.*, 1998, **95**, 6762-6767.
46. B. Birdsall, R. W. King, M. R. Wheeler, C. A. Lewis, Jr., S. R. Goode, R. B. Dunlap and G. C. K. Roberts, *Anal. Biochem.*, 1983, **132**, 353-361.
47. J. R. Lakowicz, *Principles of Fluorescence Spectroscopy*
3rd edn., Springer, New York, 2006.
48. M. Maity, S. Das and N. C. Maiti, *Phys. Chem. Chem. Phys.*, 2014, **16**, 20013-20022.
49. R. Swaminathan, N. Periasamy, J. B. Udgaonkar and G. Krishnamoorthy, *The Journal of Physical Chemistry*, 1994, **98**, 9270-9278.
50. W. Peng, F. Ding, Y.-K. Peng and Y. Sun, *Mol. BioSyst.*, 2014, **10**, 138-148.
51. P. D. Ross and S. Subramanian, *Biochemistry*, 1981, **20**, 3096-3102.

52. R. A. Goldbeck, R. M. Esquerra and D. S. Kliger, *J. Am. Chem. Soc.*, 2002, **124**, 7646-7647.
53. A. Manna and S. Chakravorti, *Mol. BioSyst.*, 2013, **9**, 246-257.
54. D. Patra and A. K. Mishra, *TrAC Trends in Analytical Chemistry*, 2002, **21**, 787-798.
55. A. Dong, P. Huang and W. S. Caughey, *Biochemistry*, 1990, **29**, 3303-3308.
56. J. Kong and S. Yu, *Acta Biochim. Biophys. Sin.*, 2007, **39**, 549-559.
57. A. Elliott and E. J. Ambrose, *Nature (London, U. K.)*, 1950, **165**, 921-922.
58. H. Susi and D. M. Byler, *Methods Enzymol.*, 1986, **130**, 290-311.
59. G. Damian, S. Cavalu, V. Miclaus, L. Sabau, N. Vedeanu and C. M. Lucaciu, *Rom. J. Biophys.*, 2007, **17**, 139-148.
60. S. Y. Venyaminov and N. N. Kalnin, *Biopolymers*, 1990, **30**, 1259-1271.
61. T. Miyazawa, T. Shimanouchi and S. Mizushima, *J. Chem. Phys.*, 1956, **24**, 408-418.
62. J. Bandekar, *Biochim. Biophys. Acta, Protein Struct. Mol. Enzymol.*, 1992, **1120**, 123-143.
63. J. L. R. Arrondo, A. Muga, J. Castresana and F. M. Goni, *Prog. Biophys. Mol. Biol.*, 1993, **59**, 23-56.
64. P. J. Tonge, M. Pusztai, A. J. White, C. W. Wharton and P. R. Carey, *Biochemistry*, 1991, **30**, 4790-4795.
65. P. J. Tonge, R. Fausto and P. R. Carey, *J. Mol. Struct.*, 1996, **379**, 135-142.
66. L. H. D. a. S. E. W. Norman B. Colthup.
67. A. K. Dioumaev and M. S. Braiman, *J. Am. Chem. Soc.*, 1995, **117**, 10572-10574.
68. G. Maes and T. Zeegers-Huyskens, *J. Mol. Struct.*, 1983, **100**, 305-315.
69. G. Maes, A. Smolders, P. Vandevyvere, L. Vanderheyden and T. Zeegers-Huyskens, *J. Mol. Struct.*, 1988, **173**, 349-356.
70. P. R. Carey, *Journal of Raman Spectroscopy*, 1998, **29**, 7-14.
71. N. C. Maiti, P. R. Carey and V. E. Anderson, *J. Phys. Chem. A*, 2003, **107**, 9910-9917.
72. R. M. Badger and S. H. Bauer, *J. Chem. Phys.*, 1937, **5**, 839-851.
73. E. Lippert, *Angewandte Chemie*, 1975, **87**, 637-637.
74. H.-U. Gremlich, B. Yan and Editors, *Infrared and Raman Spectroscopy of Biological Materials. [In: Pract. Spectrosc., 2001; 24]*, Dekker, 2001.
75. R. Callender and H. Deng, *Annu Rev Biophys Biomol Struct*, 1994, **23**, 215-245.
76. A. Barth, *Biochim. Biophys. Acta, Bioenerg.*, 2007, **1767**, 1073-1101.
77. N. C. Maiti, D. Jiang, A. J. Wain, S. Patel, K. L. Dinh and F. Zhou, *J. Phys. Chem. B*, 2008, **112**, 8406-8411.
78. M. A. Williams and J. E. Ladbury, in *Protein Science Encyclopedia*, Wiley-VCH Verlag GmbH & Co. KGaA, 2008.
79. A. K. Shaw and S. K. Pal, *J. Photochem. Photobiol., B*, 2008, **90**, 187-197.

Figures

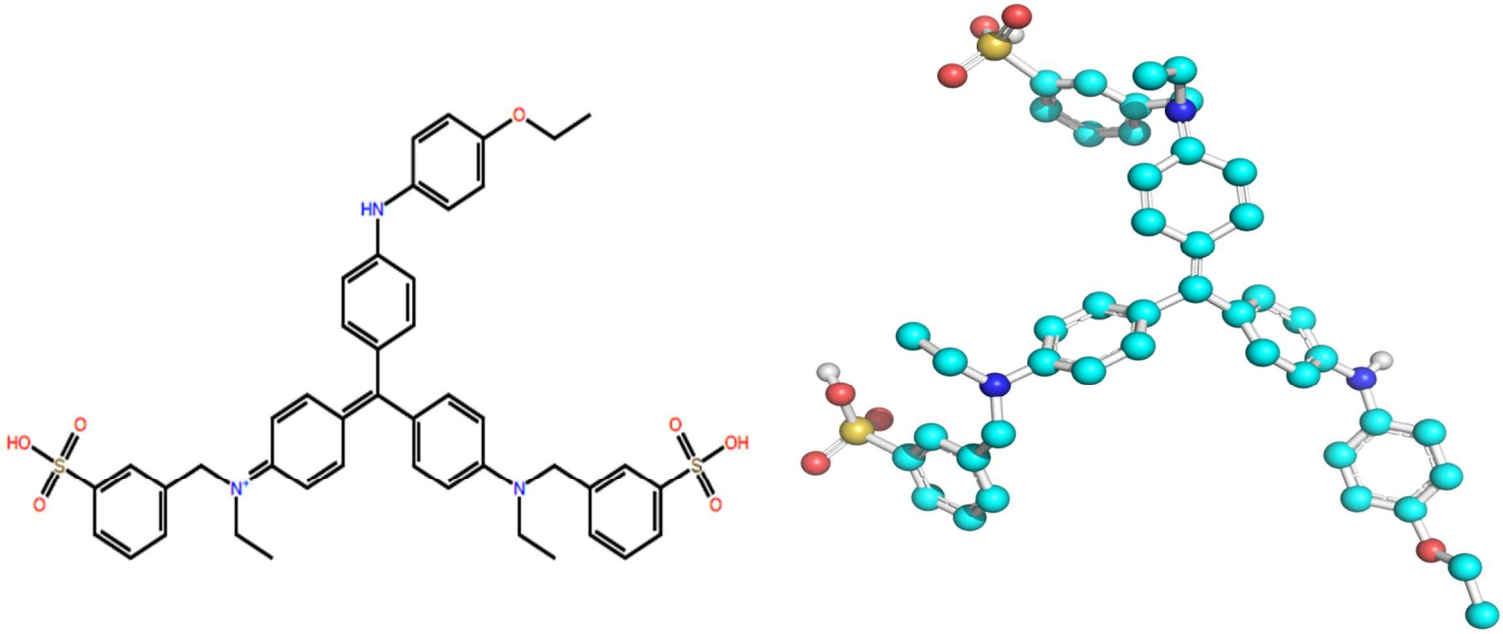

Figure 1: 2D structure of CBB-R (left) and its energy minimized 3D structure using the Gaussian 09 program . This structure was used in molecular docking and dynamic study (right).

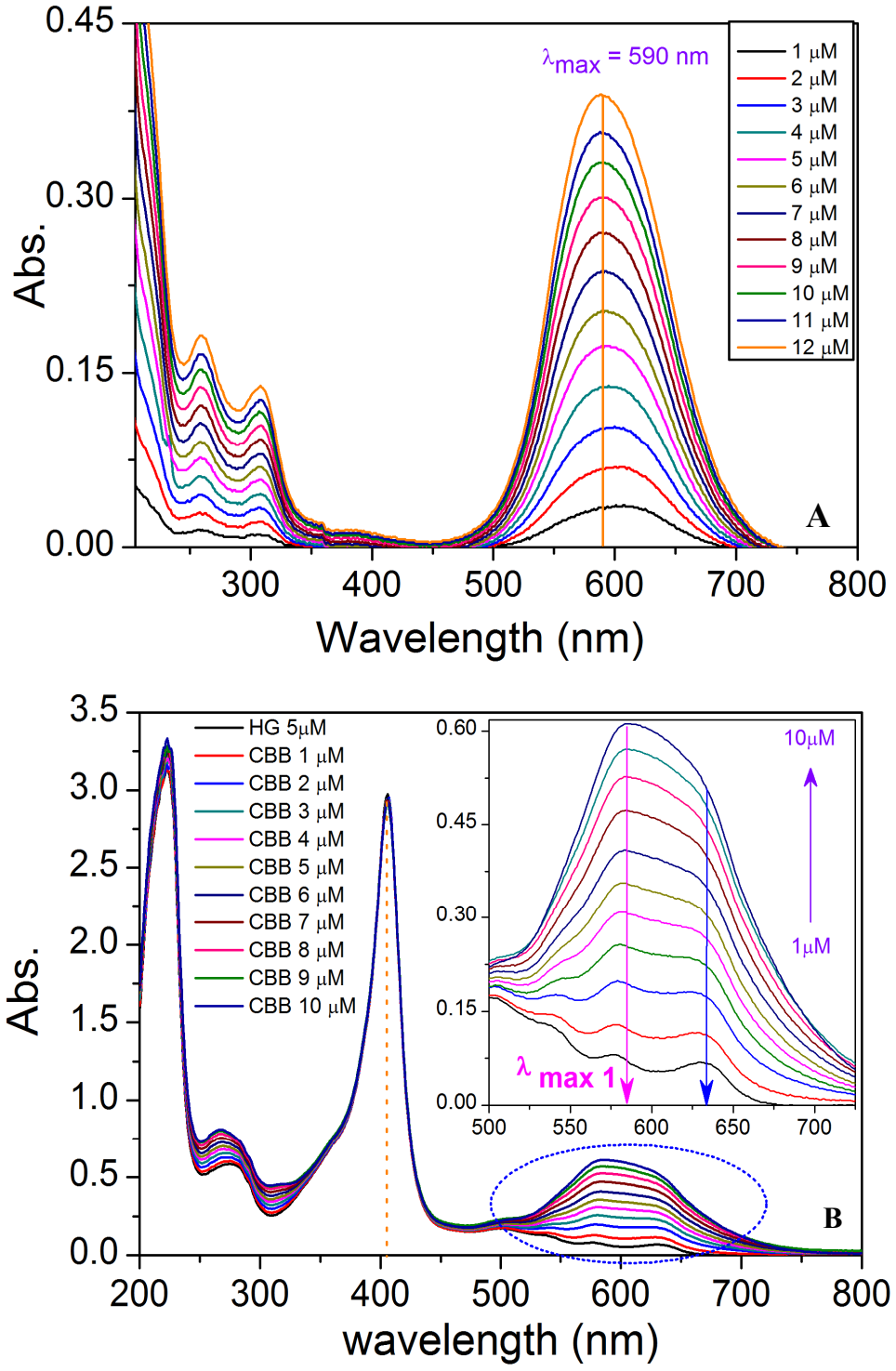

Figure 2: Panel A. UV-Vis spectrum of CBB-R in 5mM phosphate buffer at pH 7.4. The spectra were recorded in different concentration of molecules and they were labeled accordingly. Panel B. Fluorescence spectra of BHG (5μM) in the presence of different concentration of CBB-R. Inset in the panel B shows an expanded UV-Vis spectrum in the region 500 to 750 nm.

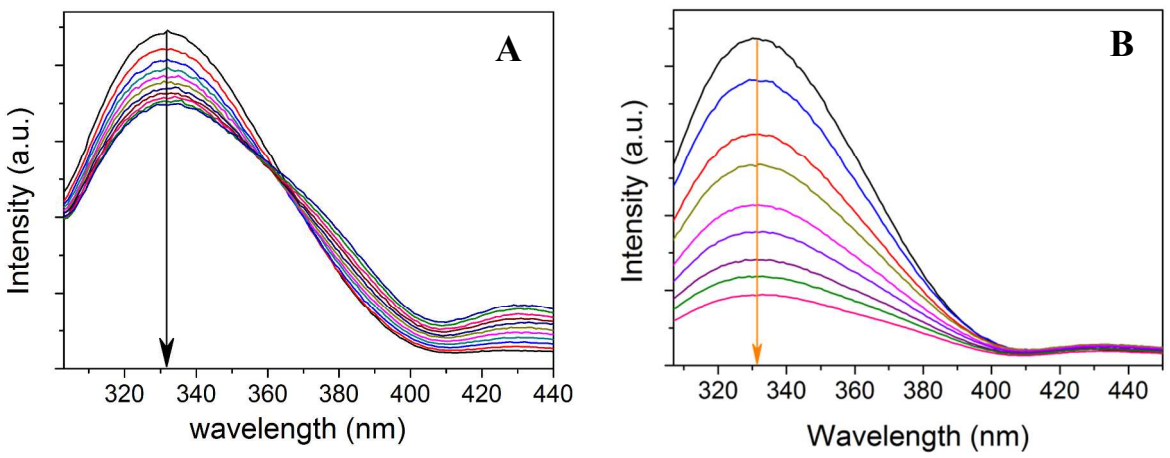

Figure 3: Change of fluorescence of BHG (5.0 μM) in 10.0 mM phosphate buffer solutions upon the addition of different concentration of CBB-R at pH 7.4 at 37 ^{o}C. The concentration of CBB-R was varied from 0.125 μM to 2.0 μM.with the increase of CBB-R concentration the intrinsic fluorescence intensity of BHG decreases. The excited wavelength (λ_{ex}) was 290 nm and the path length of the cell/cuvette was 10 mm. The panel A indicates the original spectrum as given by the instrument and panel B show the normalized and inner-filter corrected (using the values of emission at 440 nm and the inner-filter correction was done using equation 1, respectively)

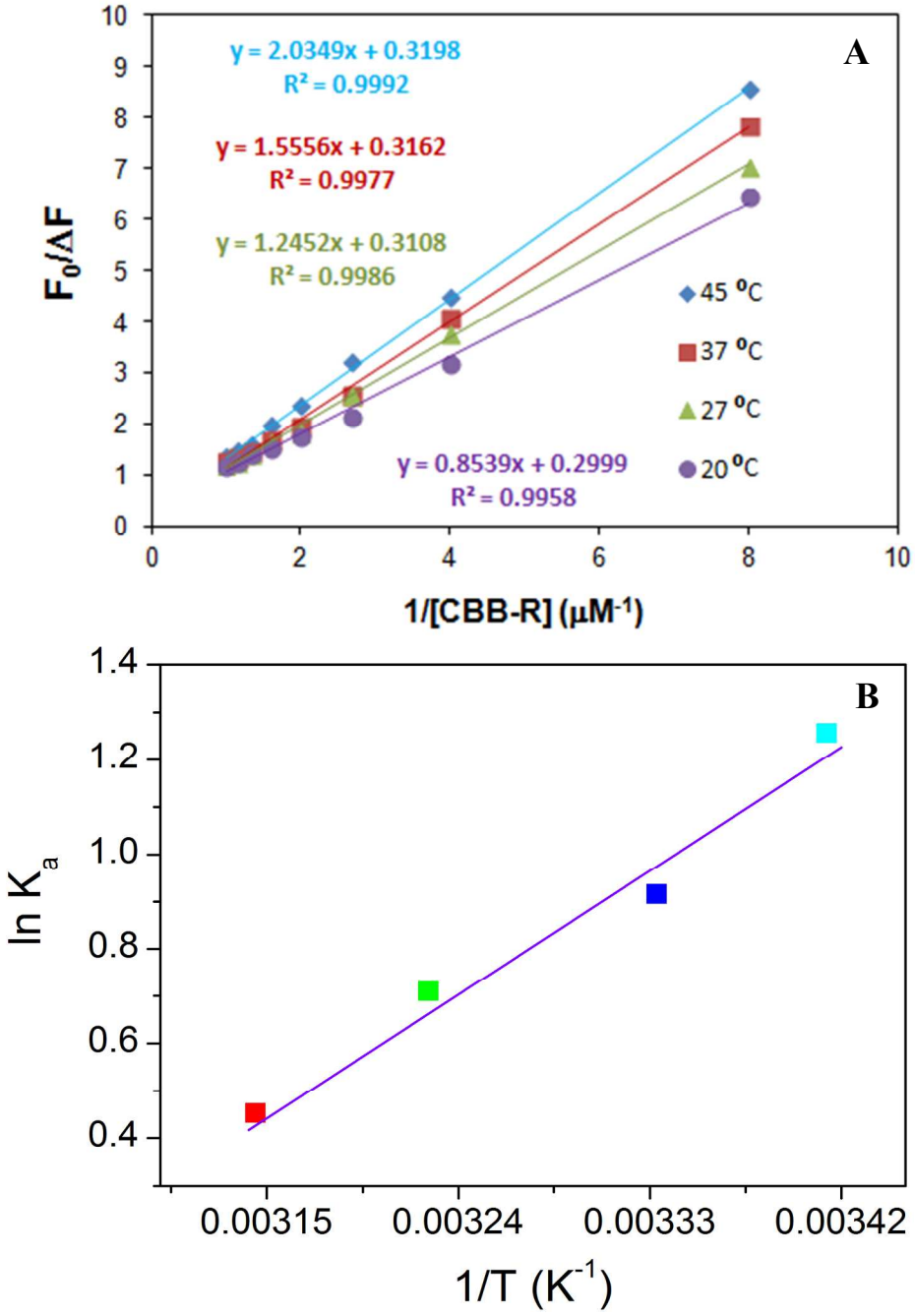

Figure 4: Panel A show the modified stern-volmer plot of fluorescence of BHG at 330 nm against reciprocal of different CBB-R concentration. The experiment was done at four different temperatures. Panel B shows van't Hoff plot of the BHG/CBB-R complex in the same buffer solution.

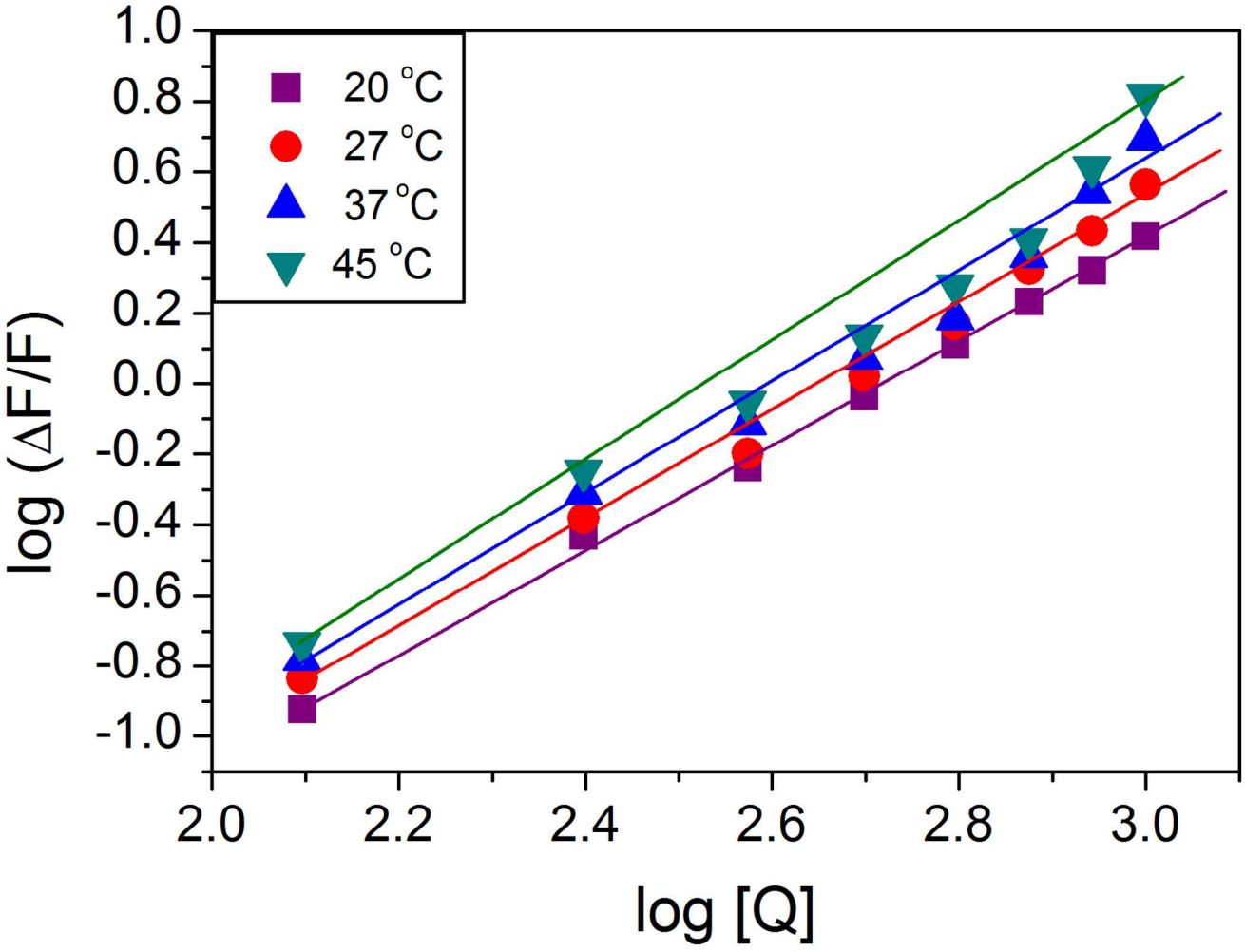

Figure 5: Determination of binding affinity constant from fluorescence data at four different temperatures.

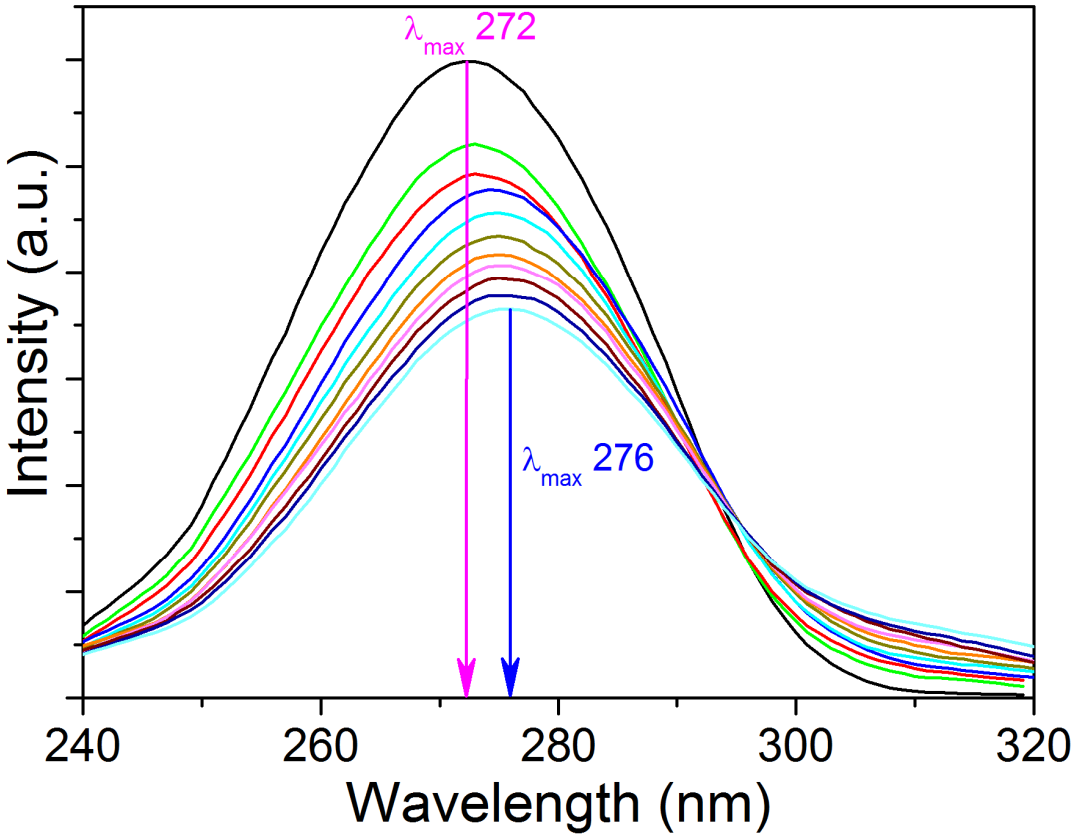

Figure 6: Synchronous fluorescence spectra (Δλ = 60 nm) of BHG (5.0 μM) in the presence of the different concentration of CBB-R in 5.0 mM phosphate buffer solution at pH 7.4

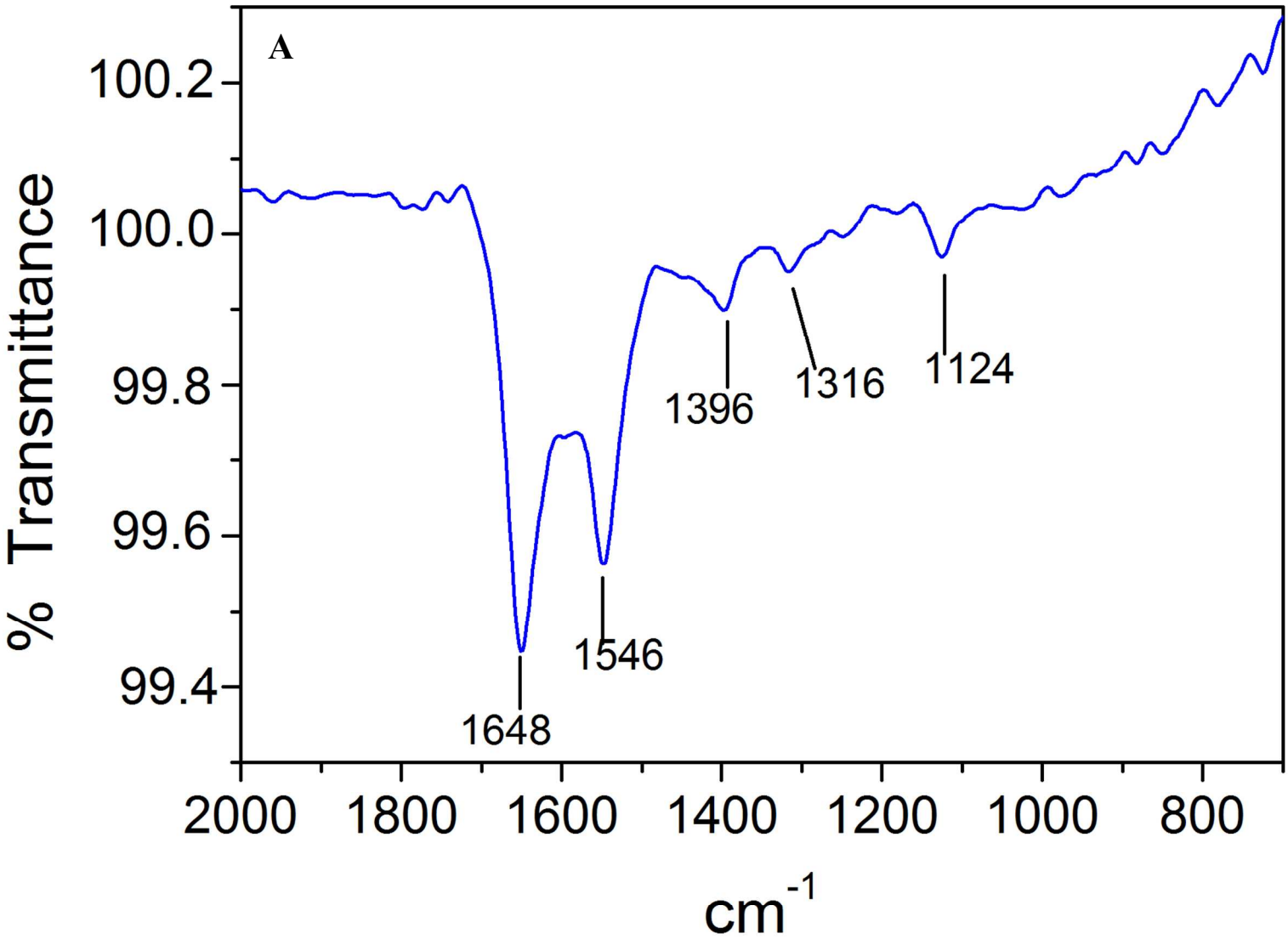

Figure 7A: The expanded FT-IR spectrum of BHG (10.0 μM) in aqueous phosphate buffer solution.The spectrum in figure S6 panel A was expanded in the region 2000 to 700 cm^{-1}.

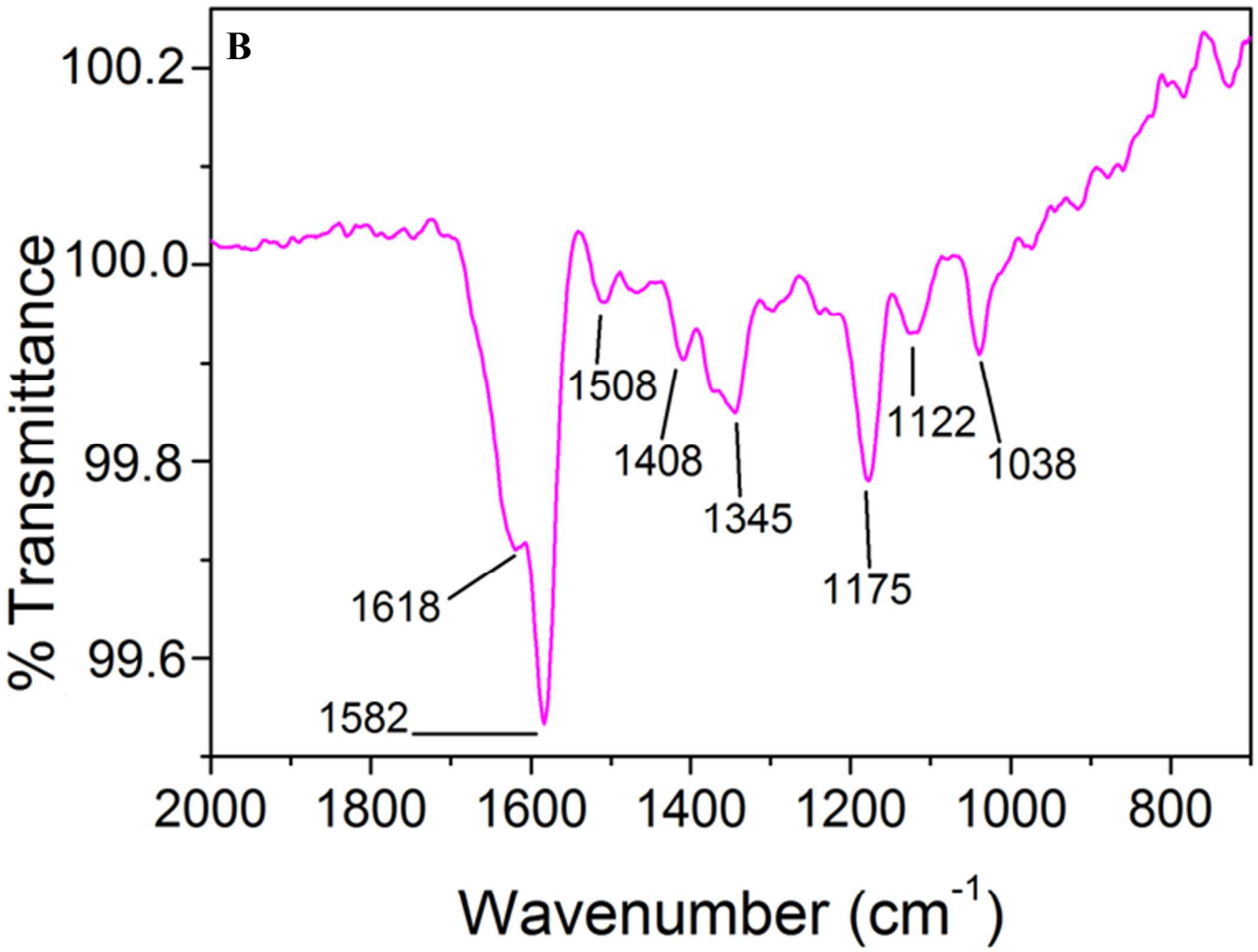

Figure 7B: The expanded FT-IR spectrum of CBB-R (20.0 μM) in aqueous phosphate buffer solution. The spectrum in figure S6 panel B was expanded in the region 2000 to 700 cm^{-1}.

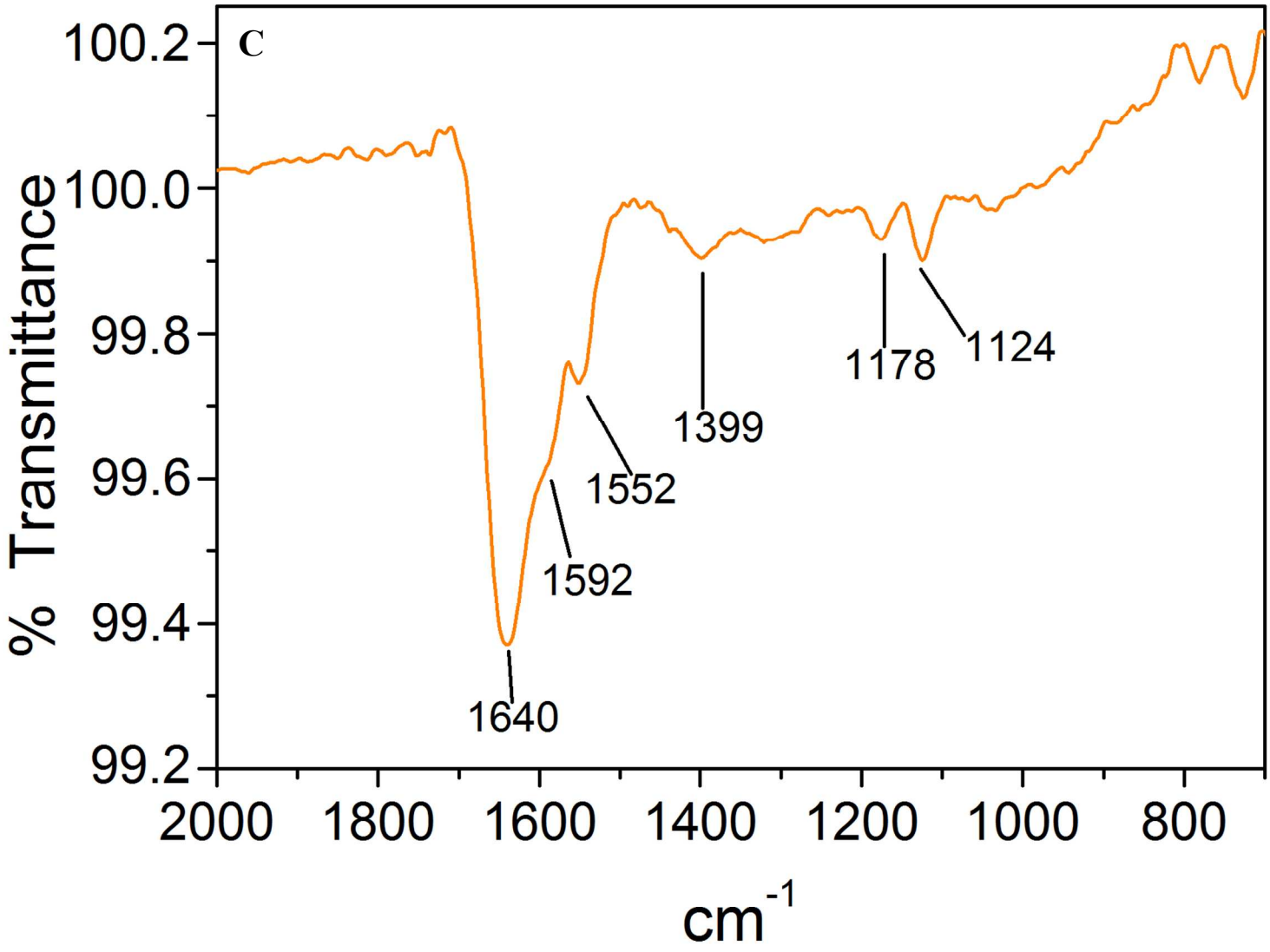

Figure 7C: The expanded FT-IR spectrum of BHG (10μM) in the presence of CBB-R (7.5 μM). The spectrum in figure S6 panel C was expanded in the region 2000 to 700 cm^{-1}.

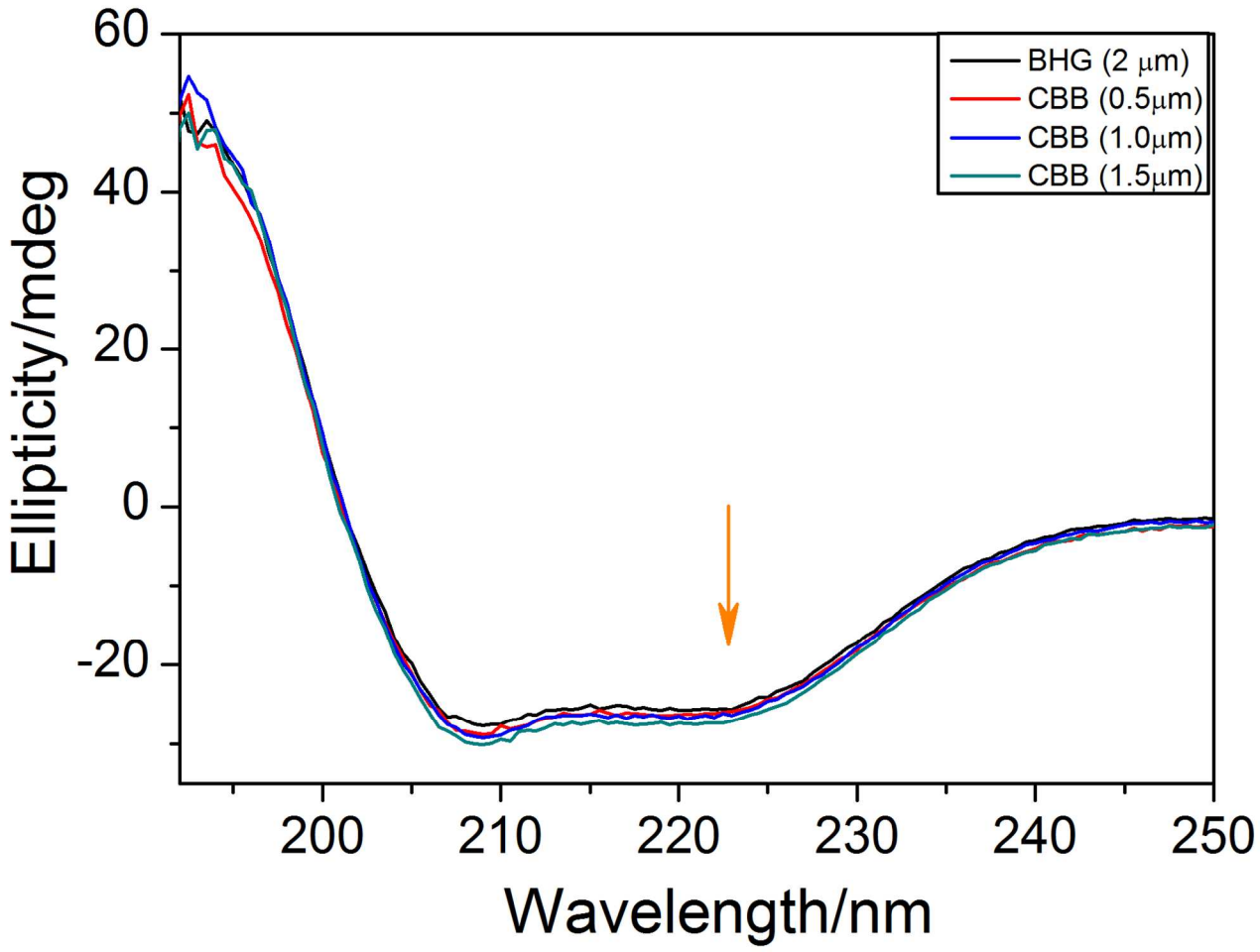

Figure 8: Circular dichroism (CD) spectra of BHG (2.0 μM) in 2.0 mM phosphate buffer solution and in the presence of different concentration of CBB-R in protein solution at 25 ^{o}C.

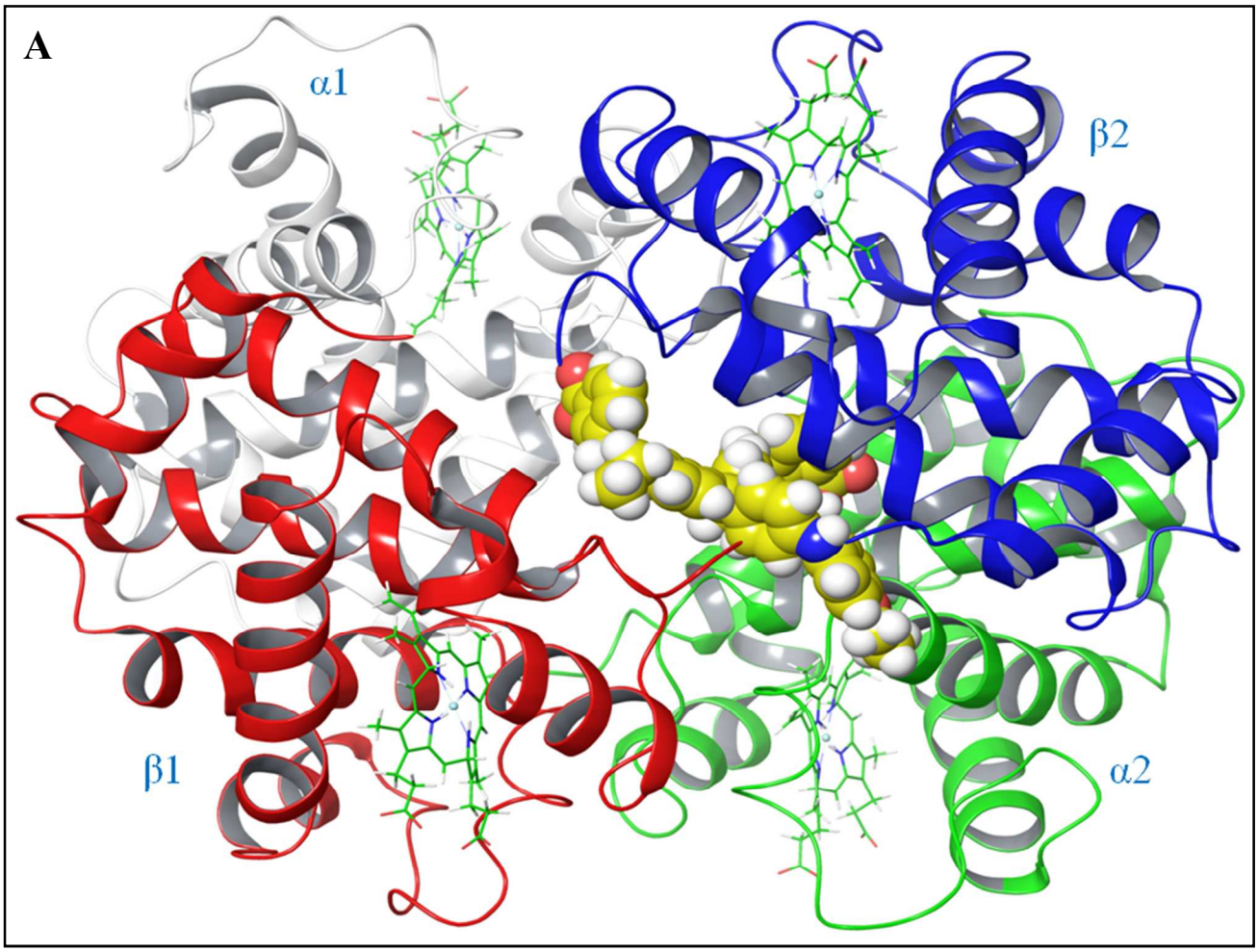

Figure 9A: The docking conformation of BHG/CBB-R complex. The image shows docked CBB-R into cavity of bovine hemoglobin, four subunits; each subunit of BHG is colored differently (white α1, red β1, green α2, and blue β2. CBB-R is colored as per atom and processes sphere (carbon atom yellow, oxygen atom red, nitrogen blue and hydrogen atom white in colour).

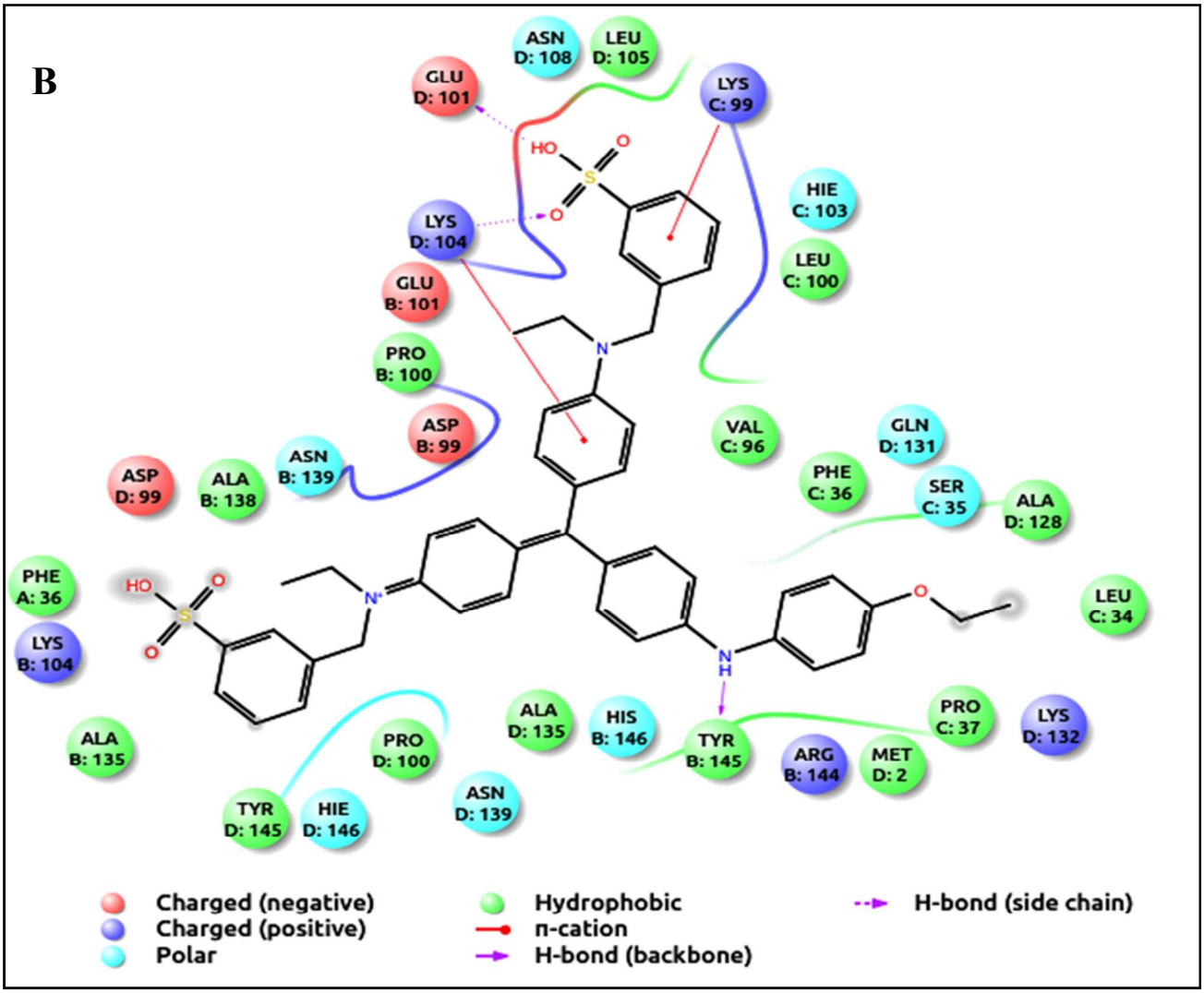

Figure 9B: 2D plot of best docking conformation observed during docking simulation. The three H-bonds between β2 subunit of Lys104, Glu101, β1 subunit of Tyr145, and two π-cation interaction between α2 subunit of Lys99 and β2 subunit of Lys104 (the notation as A, B, C and D below the three letter code of amino acids indicates α1, β1, α2 and β2 subunit, respectively).

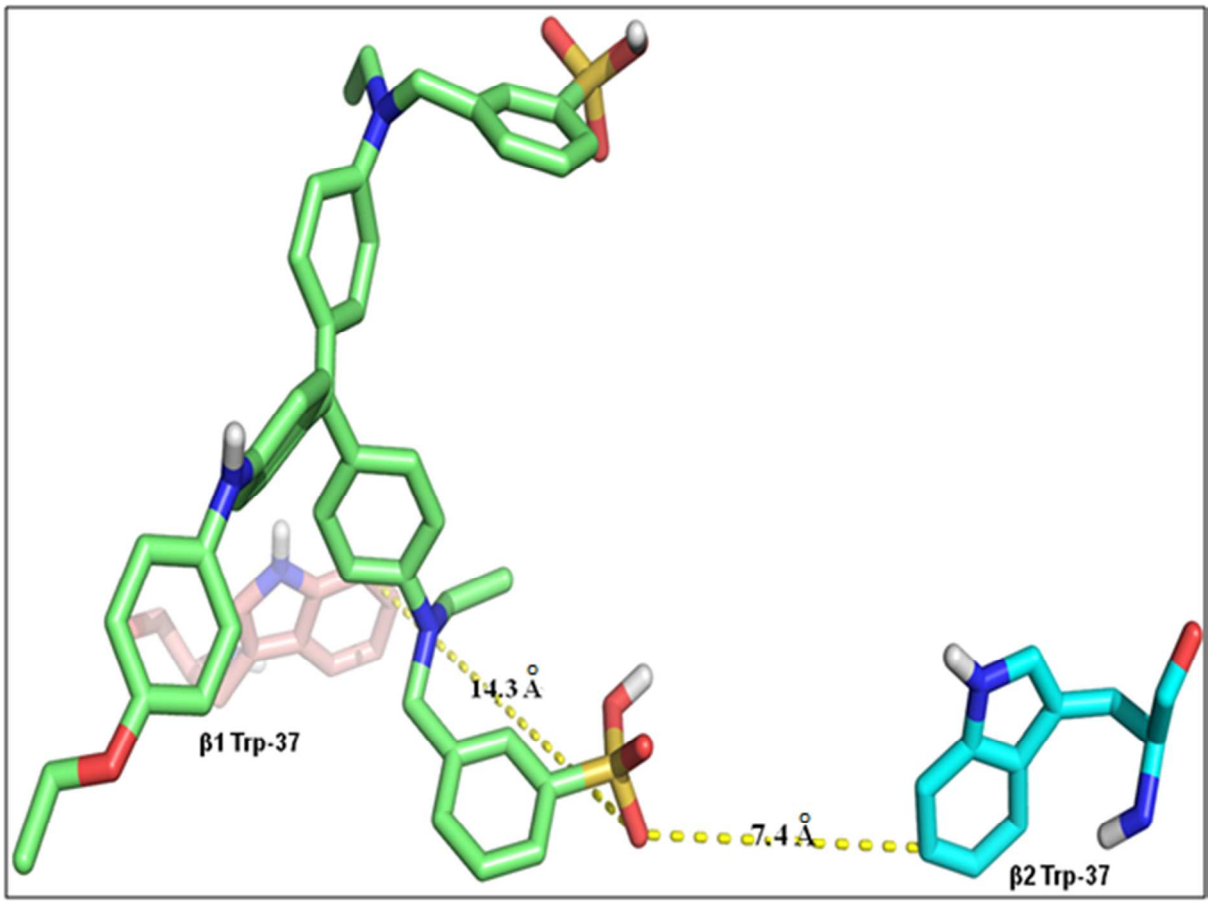

Figure 10: The distance between β1 Trp37 and β2 Trp37 of BHG with CBB-R in the best docking conformation. The presentation was made by pymol and it shows the stick model.

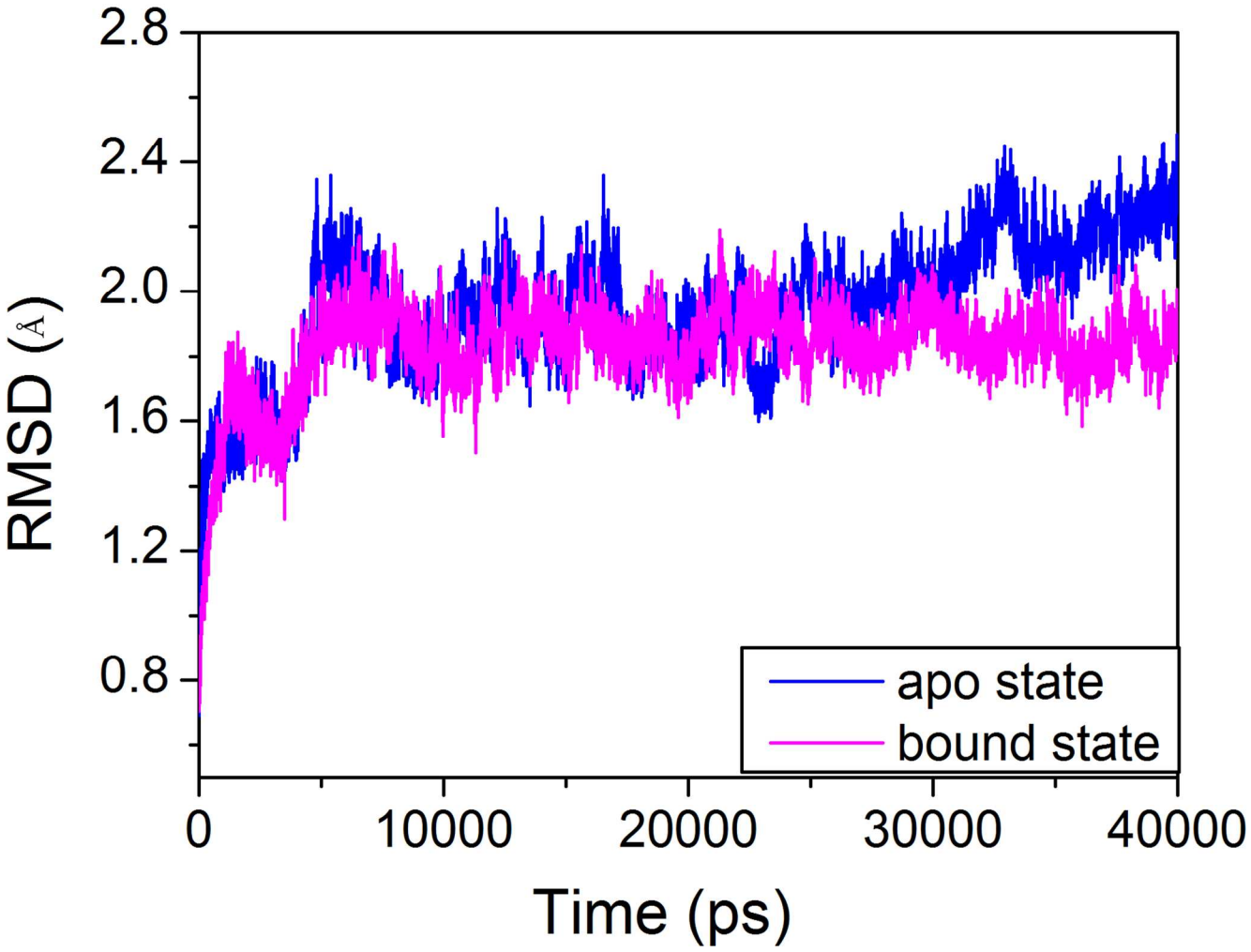

Figure 11: RMSD plot for the backbone of BHG (blue) and backbone of BHG when it forms complex with CBB-R (pink) during 40000 ps MD simulation.

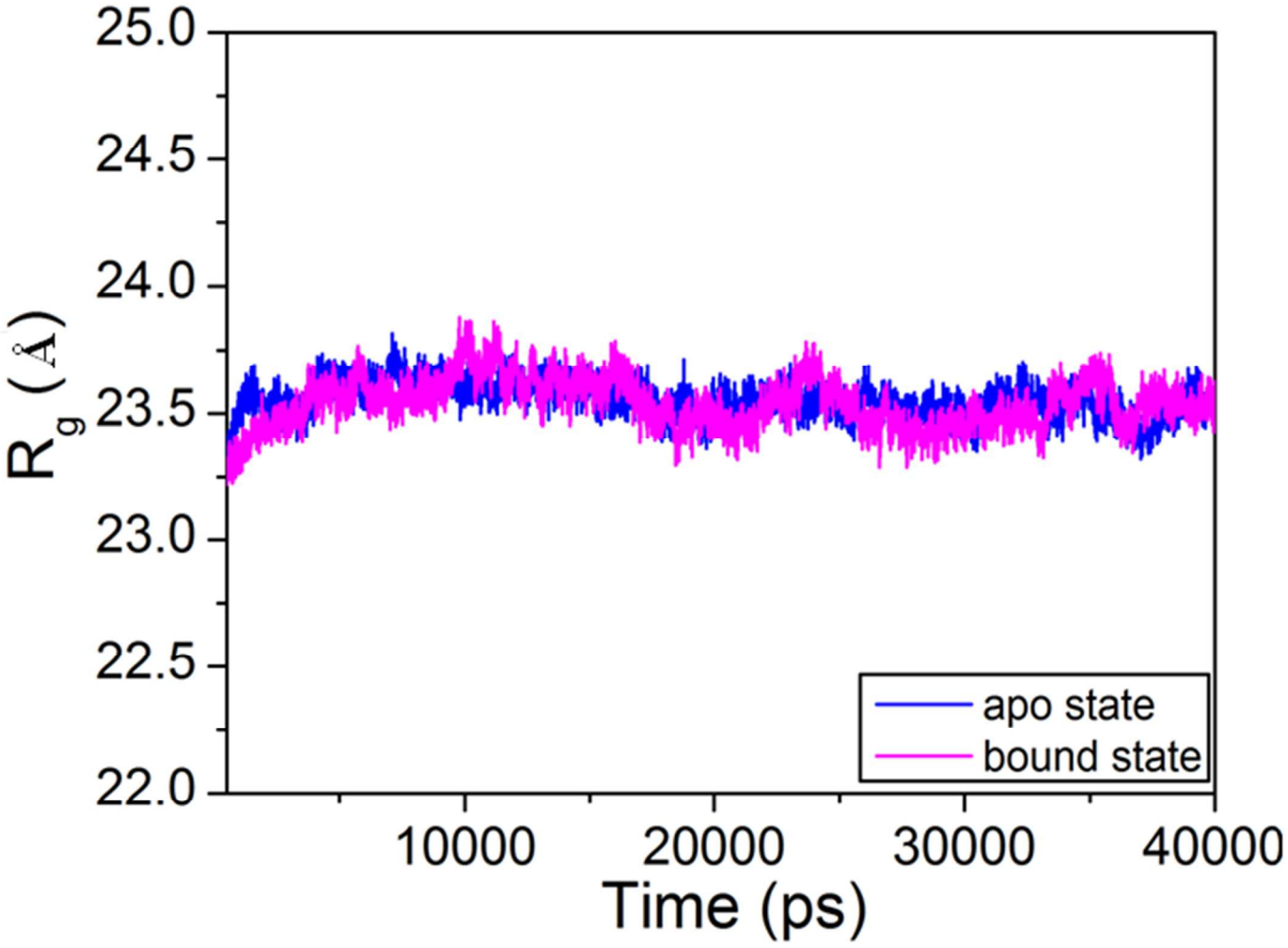

Figure 12: Change in radius of gyration of BHG (blue) and BHG/CBB-R complex (red) during 40000 ps MD simulation.

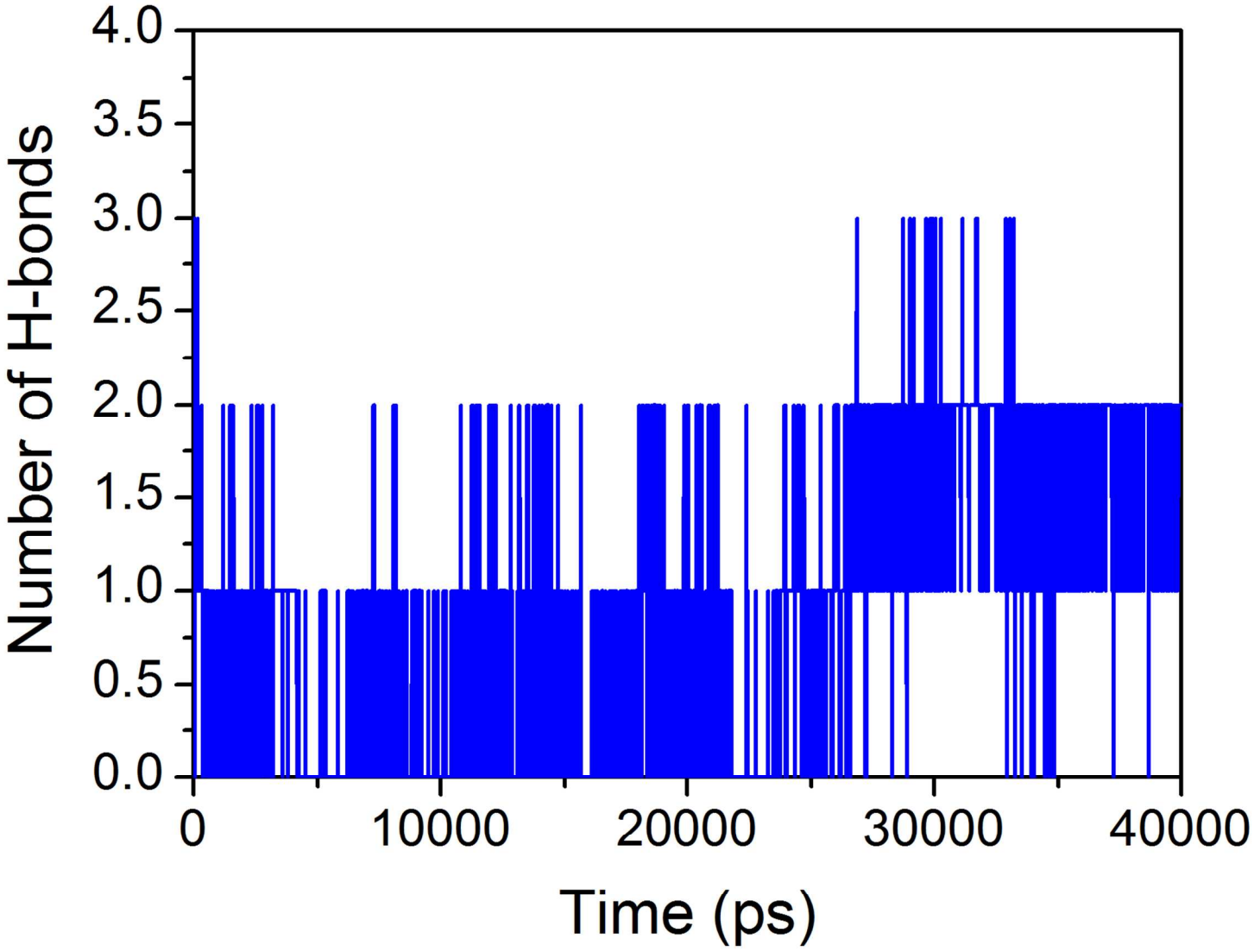

Figure 13: The H-bond interaction pattern of BHG/CBB-R complex during the molecular dynamic analysis for 40000 ps.

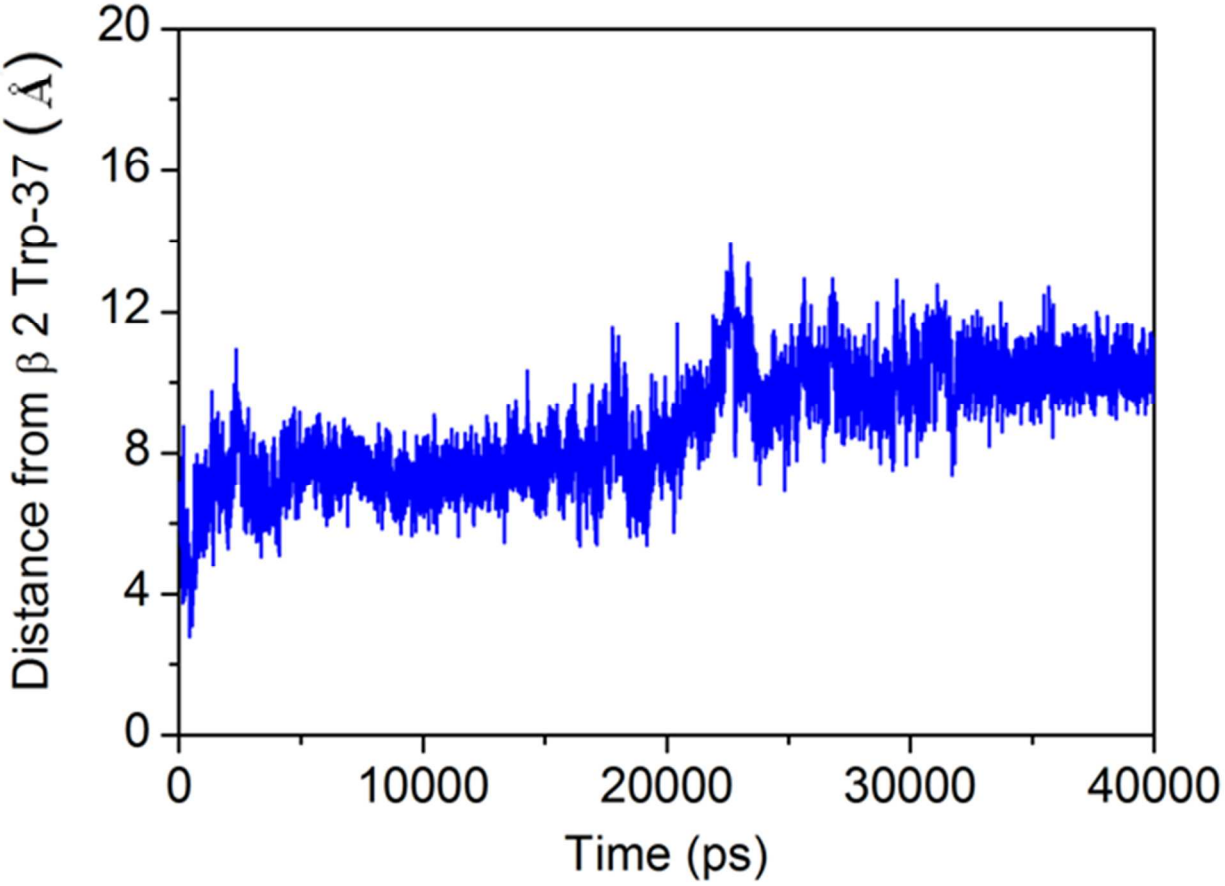

Figure 14: Minimum distance between CBB-R and Trp37 during 40000 ps MD simulation.

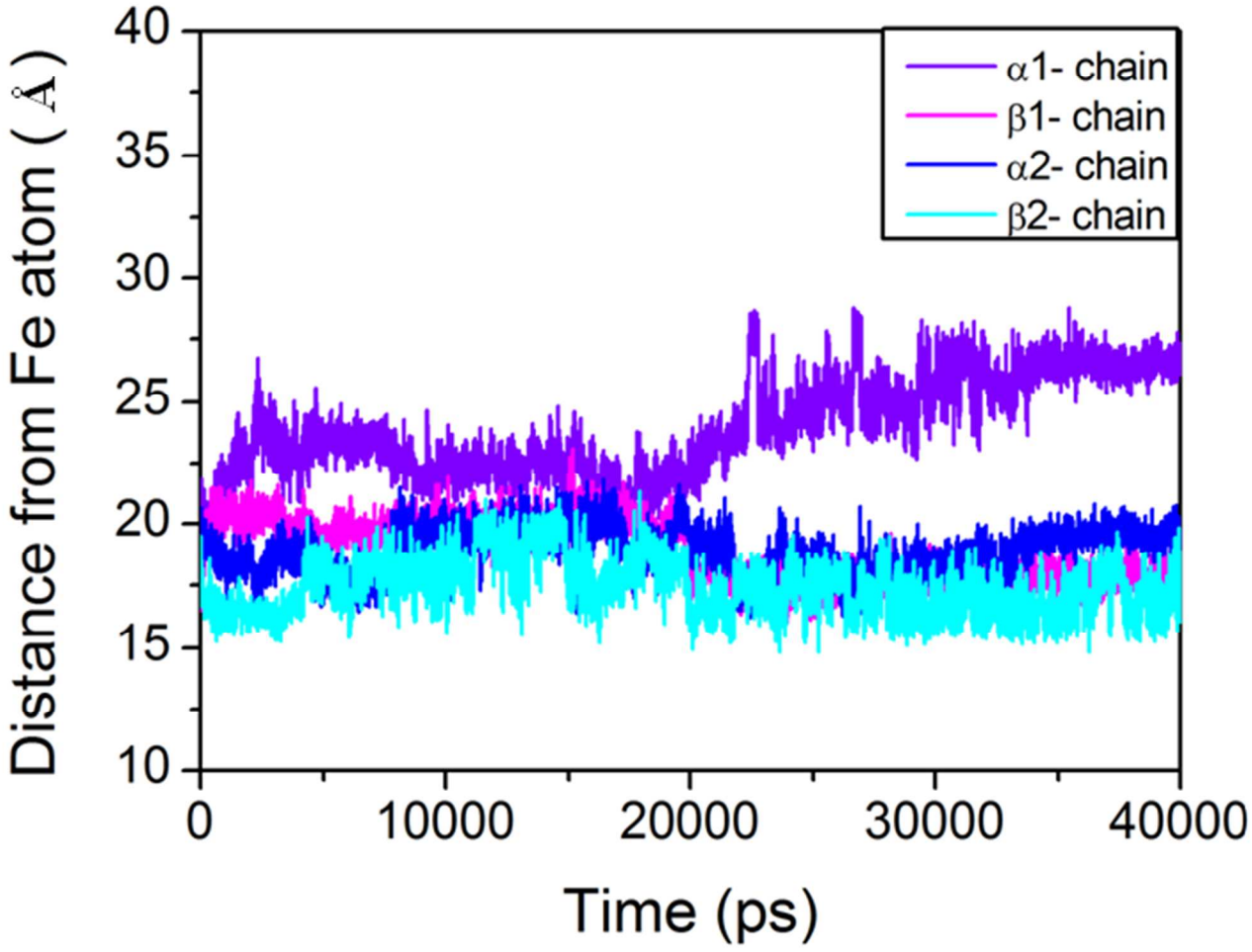

Figure 15: Minimum distance between CBB-R and four Fe atoms in heme center of BHG during 40000 ps MD simulation.